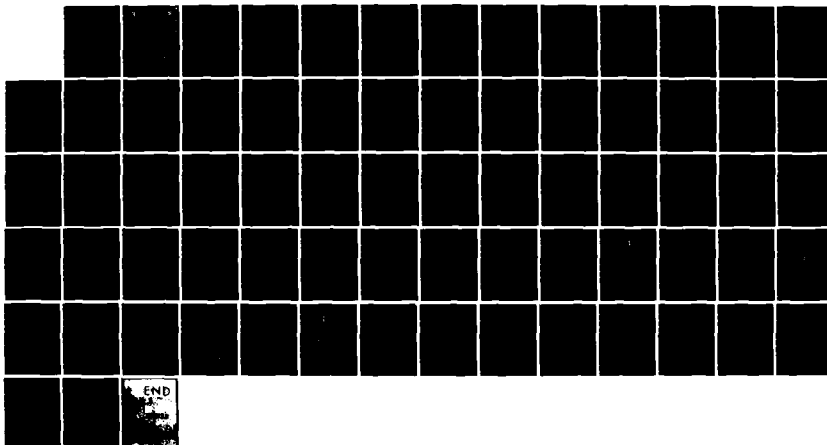
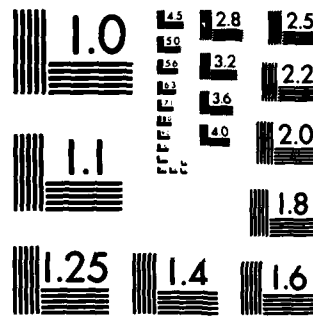


AD-A145 070 DYNAMICS OF LIQUID DROPLETS IN THE SPACE ENVIRONMENT 1/1
(U) UNIVERSITY OF SOUTHERN CALIFORNIA LOS ANGELES DEPT
OF AEROSPACE ENGINEERING E P MUNTZ ET AL. AUG 84

UNCLASSIFIED AFRPL-TR-84-045 F04611-82-K-0040 F/G 20/4 NL





MICROCOPY RESOLUTION TEST CHART
NATIONAL BUREAU OF STANDARDS-1963-A



AFRPL TR-84-045

AD:



Final Report
for the period
10 May 1982 to
30 September 1983

Dynamics of Liquid Droplets in the Space Environment

August 1984

Authors:
E. P. Muntz
M. Dixon

University of Southern California
Department of Aerospace Engineering
University Park
Los Angeles, CA 90009

F04611-82-K-0040

Subject to Export Control Laws

This document contains information for manufacturing or using munitions of war. Exporting this information or releasing it to foreign nationals living in the United States without first obtaining an export license violates the International Traffic in Arms Regulations. Under 22 USC 2778, such a violation is punishable by up to 2 years in prison and by a fine of \$100,000.

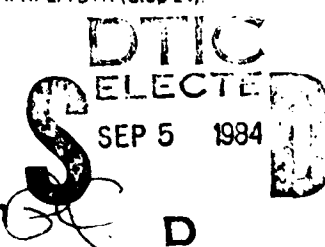
Distribution limited to U.S. Government agencies and their contractors only. Critical Technology. August 1984. Other requests for this document must be referred to AFRPL/TSTR (Stop 24). Edwards AFB, CA 93523

AD-A145 070

DTIC FILE COPY

prepared for the: Air Force
Rocket Propulsion
Laboratory

Air Force Space Technology Center
Space Division, Air Force Systems Command
Edwards Air Force Base,
California 93523



84 08 31 029

SECURITY CLASSIFICATION OF THIS PAGE

REPORT DOCUMENTATION PAGE

1a. REPORT SECURITY CLASSIFICATION Unclassified		1b. RESTRICTIVE MARKINGS										
2a. SECURITY CLASSIFICATION AUTHORITY		3. DISTRIBUTION/AVAILABILITY OF REPORT Distribution limited to U.S. Government agencies and their contractors only; Critical Technology, August 1984. Other requests										
2b. DECLASSIFICATION/DOWNGRADING SCHEDULE												
4. PERFORMING ORGANIZATION REPORT NUMBER(S)		5. MONITORING ORGANIZATION REPORT NUMBER(S) AFRPL-TR-84-045										
6a. NAME OF PERFORMING ORGANIZATION University of Southern Calif.	6b. OFFICE SYMBOL (If applicable)	7a. NAME OF MONITORING ORGANIZATION Air Force Rocket Propulsion Laboratory										
6c. ADDRESS (City, State and ZIP Code) University Park Los Angeles CA 90089-1454		7b. ADDRESS (City, State and ZIP Code) AFRPL/DYSS, Stop 24 Edwards Air Force Base, CA 93523										
8a. NAME OF FUNDING/SPONSORING ORGANIZATION	8b. OFFICE SYMBOL (If applicable)	9. PROCUREMENT INSTRUMENT IDENTIFICATION NUMBER F04611-82-K-0040										
8c. ADDRESS (City, State and ZIP Code)		10. SOURCE OF FUNDING NOS. PROGRAM ELEMENT NO. PROJECT NO. TASK NO. WORK UNIT NO. 61101F 3058 00 AX										
11. TITLE (Include Security Classification) DYNAMICS OF LIQUID DROPLETS IN THE SPACE...												
12. PERSONAL AUTHOR(S) E.P. Muntz, Melissa Dixon												
13a. TYPE OF REPORT Final	13b. TIME COVERED FROM 82/5/10 TO 83/9/30	14. DATE OF REPORT (Yr., Mo., Day) 84/8	15. PAGE COUNT 71									
16. SUPPLEMENTARY NOTATION												
17. COSATI CODES <table border="1"><tr><th>FIELD</th><th>GROUP</th><th>SUB. GR.</th></tr><tr><td>21</td><td>08</td><td></td></tr><tr><td></td><td></td><td></td></tr></table>		FIELD	GROUP	SUB. GR.	21	08					18. SUBJECT TERMS (Continue on reverse if necessary and identify by block number) Droplet streams, angular and speed coherence of droplet streams, droplet propagation in space, liquid droplet radiator	
FIELD	GROUP	SUB. GR.										
21	08											
19. ABSTRACT (Continue on reverse if necessary and identify by block number) This report discusses the angular and speed dispersions of streams of liquid droplets in a high vacuum. Measurements of angular and speed dispersions of several droplet streams of low pressure liquids are reported. The results are interpreted with reference to proposed physical mechanisms for generating the observed dispersions. Typically, angular dispersions are around $2\mu\text{rad}$ and speed dispersions around 1.5×10^{-5} of the stream average speed. An addendum to the report discusses the results relative to proposed Air Force system uses.												
20. DISTRIBUTION/AVAILABILITY OF ABSTRACT UNCLASSIFIED/UNLIMITED <input checked="" type="checkbox"/> SAME AS RPT. <input type="checkbox"/> DTIC USERS <input type="checkbox"/>		21. ABSTRACT SECURITY CLASSIFICATION Unclassified										
22a. NAME OF RESPONSIBLE INDIVIDUAL Michael Riffle, 2Lt, USAF		22b. TELEPHONE NUMBER (Include Area Code) (805) 277-5147	22c. OFFICE SYMBOL DYSS									

SECURITY CLASSIFICATION OF THIS PAGE

Block 3: for this document must be referred to AFRPL/TSTR, Stop 24, Edwards Air Force
Base, CA 93523.

Block 11: ENVIRONMENT (U)

SECURITY CLASSIFICATION OF THIS PAGE

Table of Contents

1. Introduction	4
2. Facility and Instrument Design	4
2.1. General	4
2.2. Droplet Dynamics Space Simulator	7
2.3. Droplet Generator	8
2.4. Instrumentation	10
2.4.1. Droplet Visualization	10
2.4.2. Direct Measurement of Angular Spread	11
2.4.3. Droplet Velocimeter	12
3. Nozzle and Stream Fluid Mechanics	13
3.1. Nozzle Configuration	13
3.2. Droplet Formation	14
3.3. Droplet Propagation	17
3.3.1. Introduction	17
3.3.2. Estimate of the Order of Magnitude of Droplet Velocity Perturbations	19
3.3.3. External Forces on the Stream at the Nozzle Exit	21
3.3.4. Relationship Between Stream Radius Perturbation and Stagnation Pressure Changes	21
3.4. Droplet Impact on Liquid and Dry Surfaces	22
4. Results	23
4.1. Average Stream Speeds	24
4.2. Angular and Speed Dispersions	24
4.3. Stream Charging	29
4.4. Droplet Impact Experiments	30
5. Conclusions	31

Accession For	
NTIS CRA&I	<input type="checkbox"/>
DTIC TAB	<input checked="" type="checkbox"/>
Unannounced	<input type="checkbox"/>
Justification	
By _____	
Distribution/	
Availability Codes	
Dist	Avail and/or Special
C/2	



Symbols

C^*	Capillary number, W^*/Re^*
d	Droplet diameter
D	Nozzle diameter
D_0	Liquid column diameter
D_s	Stationary diameter of droplet on surface
$d\theta$	Angular deviation of stream
dV	Axial speed deviation of stream
F	Droplet spread factor
f	Applied disturbance frequency
f_c	Cut-off frequency
F_1	Perpendicular force on stream at nozzle exit
F_z	Parallel force on stream at nozzle exit
K	Constant approximately equal to 20
K'	Number of characteristic times required for break-up
K_L	Constant to account for entrance effect due to shear (equal to 1.3)
k_o^*	Nondimensional wave number
L	Nozzle length
l	Droplet separation
L_e	Entrance length before fully developed Poiseuille flow
L_f	Flight path length
m	Molecular weight
M_d	Mass of droplet

n	Number density
n_{\max}	Maximum number density
P_d	Droplet momentum
p_s	Stagnation pressure
P_F	Flight tube pressure
Re_d	Reynolds number based on droplet diameter
$r(Z,t)$	Radial displacement describing surface profile of stream
r_m	Maximum displacement at stream surface
R_0	Column radius
s_0	Break-up distance
T_F	Droplet flight time
t_c	Characteristic time
t_o	Minimum break-up time
$u(Z,t)$	Average perturbation flow speed in z direction
v	Stream speed
v_d	Droplet speed
v_o	Average stream speed
w^*	Weber number
Δl	Change in droplet separation
ΔM_d	Change of mass of droplet
Δp	Pressure drop across the nozzle
$\Delta P(Z_B,t)$	Total perturbation momentum
Δv_d	Change in droplet speed

ϵ^*	Amplitude of initial disturbance
λ	Wavelength of disturbance
λ^*	Nondimensional wavelength of disturbance
λ_c	Minimum or cut-off wavelength
ρ	Density of fluid
σ	Surface tension of fluid
$\sigma(\Delta\ell)$	Standard deviation of change in droplet spacing
$\sigma(\Delta V_d)$	Standard deviation of change in droplet speed
σ_L	Surface tension liquid
σ_{LS}	Surface tension at liquid-solid interface
σ_S	Surface tension of solid
$\sigma(\Delta\theta)$	Standard deviation of angular dispersion
θ_c	Contact angle
μ	Coefficient of viscosity of fluid

1. Introduction

There are a number of applications in space for well controlled streams of liquid droplets. These include; the liquid droplet radiator concept (Ref. 1), transport of consumables between spacecraft (Ref. 2) and space construction applications (Ref. 2). For all of these possible uses basic information on the direction and speed control of droplet streams in the space environment is required over a wide range of; droplet size, droplet speed, liquid viscosity, surface tension and orifice or nozzle geometry.

There is some evidence that droplet streams can achieve a rather remarkable coherence (Ref. 3). This report describes the results of a one-and-a-half year program at the University of Southern California to investigate the limits of droplet stream coherence in a high vacuum. The study involved the design and construction of a facility that has the high inertial stability, vacuum capability and relatively long flight paths that are required. A series of measurements of droplet stream angular and speed dispersion have been made for a range of droplet diameters, using several types of liquid.

2. Facility and Instrument Design

2.1. General

It appeared that angular dispersions of the order of microradians could be achieved by droplet streams in a vacuum. The apparatus constructed for this investigation had, as a primary design goal, an ability to measure droplet stream angular dispersion with a resolution better than 1 microradian. While there are other requirements, the angular resolution was the one that dominated the design. Consider a nominal $100\mu\text{m}$ diameter droplet stream, the deviation corresponding to 1 μrad at the end

of a 10 m flight is 10^{-1} diameters (or 10μ). A measurement of about 10^{-1} diameters was considered to be a reasonable lower limit that might be achieved with relatively little effort, since the position of a droplet must be specified by the droplet image. With greater care displacements of 10^{-2} droplet diameters could be determined, but this requires careful and time consuming image analysis, as well as very good images. As a result of these considerations a flight path on the order of 10 m is required.

If the flight path is to be effectively at space conditions or space vacuum, the residual gas should represent a negligible disturbance to the flight of the droplets (consideration of droplet streams at low Earth orbital altitudes is outside the scope of the present program). If we say that there should be no gas disturbance that represents greater than one part in 10^6 speed disturbance to the droplets, we can estimate the required gas number density by calculating the momentum swept by a droplet. Say a droplet of diameter d and density ρ travels at a speed V_d in a gas of molecular weight m and number density n . The momentum defect is approximately,

$$(\pi/4)d^2mV_d n L_F \quad (1)$$

for a flight path length L_F .

We require this to be 10^{-6} of the droplet momentum and thus the maximum allowable number density in the flight tube is

$$n_{max} = (2/3)(\rho d / mL_F) \cdot 10^{-6} \quad (2)$$

For: $\rho = 1 \text{ gm/cm}^3$, $d = 0.01 \text{ cm}$, $L_F = 10^3 \text{ cm}$ and assuming nitrogen is the residual gas the maximum number density is $2 \times 10^{12} \text{ cm}^{-3}$, which corresponds to about 10^{-4} torr. For $10\mu\text{m}$ droplets the maximum pressure is 10^{-5} torr.

The general features of a laboratory facility for measuring droplet streams with resolutions corresponding to microradian angular dispersion and microfraction speed dispersion is now clear. A flight path length approaching 10 m with a pressure of 10^{-4} torr or less is required. It is possible that surface effects due to absorbed molecular layers could be important in some droplet studies, in this situation considerably lower pressures than 10^{-4} torr would be required. Some provision should be made for this possibility. The entire facility should be inertially stabilized to better than $1\mu\text{rad}$, at least over a period of a number of droplet flight times ($<0.1\text{s}$). Because of gravitational deflection considerations it is most convenient to have the flight path parallel or anti-parallel to the gravitational vector. Assuming the alignment can be maintained to within about ± 0.1 degrees of the g vector, gravitational acceleration perpendicular to the stream is of the same order of magnitude as the coriolis acceleration (10^{-3}g). This corresponds to about a 5×10^{-6} rad stream displacement, but since both of these accelerations are constant to much better than one part in 10^{-3} there should be no measurable angular dispersion introduced from these sources. In addition to the inertial stabilization there is also a somewhat higher frequency vibration requirement that might be of concern. Capillary streams, from which the droplets are formed, are sensitive to low frequency vibration (10^2 to 10^4 Hz). The facility should be free from significant vibrational amplitudes in the frequency range above 10^2 Hz.

A description of the details of the facility which has been designed to meet the requirements presented above appears below. This in turn is followed by descriptions of the instruments that have been designed to obtain the angular and speed dispersion measurements.

2.2. Droplet Dynamics Space Simulator

The Droplet Dynamics Space Simulator (D^2S^2) is essentially a 5.5 m long, 0.25m diameter stainless steel tube attached to a 4 ft. wide 18 ft. long optical bench. The entire apparatus is suspended in a vertical orientation by four Newport Research pneumatic vibration isolation mounts placed at the level of the center of gravity of the suspended portion of the apparatus. Two 6 inch oil diffusion pumps are mounted on the stainless steel flight tube. Optical access is provided to the flight tube at either end. There is a platform, connected to the optical bench, that provides access to the droplet generator which is located on the upper end of the flight tube.

The flight tube, optical bench, access platform, diffusion pumps, droplet generator, droplet receiver and the instrumentation are all suspended on the vibration isolation mounts, effectively forming an inertially isolated body. The only external contact other than the mounts is through the flexible water cooling lines and the flexible vacuum backing line for the diffusion pumps. These are arranged to provide a minimum disturbance to the isolated body. In particular the backing vacuum connection is made through a T shaped fitting so that there are equal and opposite forces when a control volume envelope cuts these potential sources of loading on the isolated body.

The complete apparatus is sketched in Figure 1, indicating the position of the major components of the facility. The isolated body has a mass of about 2500 kg. The performance of the vibration isolation mounts is presented in Figure 29-1 of Ref. 2. Any high frequency components applied to the isolated body are damped due to the interior structural design of the optical bench (Ref. 4). There is provision for tethering the optical bench as a precaution against earthquake induced dislodgement of the isolated body from the vibration isolation mounts. The isolated body floats stably on its mounts and has a damping time of a few seconds. Liquid nitrogen cold traps for the diffusion pumps are

installed and can be filled using a quick release connection. One fill of the traps lasts for 3 h. With the cold traps filled the apparatus can be pumped to 2×10^{-6} torr in four or five hours. Operation is generally at 10^{-5} torr in about two hours.

2.3. Droplet Generator

The droplet generator is a Pacific Applied Research SED 101, it is shown schematically in Figure 2 and was made to our specifications. The SED 101's chief feature is that it permits the droplet liquid to be pressurized to 2000 psig, using gas pressurization. A flexible diaphragm is used to separate the high pressure gas from the liquid. This is necessary to prevent high pressure gas from being dissolved in the droplet liquid. Gas pressurization is used as it introduces very little vibrational disturbance to the apparatus. A high pressure gas reservoir is available on the isolated body so that no external gas lines are necessary during operation. The liquid reservoir shown in Figure 1 is used to outgas the working liquid to pressures as low as 10^{-5} torr.

The droplet generator can be operated completely remotely using the electrically actuated ball valves shown schematically in Figure 3. The droplet generator can be evacuated, outgassed, liquid loaded by gravity into the lower chambers of the droplet generator and pressure applied to the pressurization chamber, all by remote operation. The droplet generator is then ready for use. To operate, the No. 1 valve is actuated. Since the valve is completely immersed in liquid there is no detectable initiating shock even when operating at 2000 psig. The liquid is retained in the stagnation chamber by surface tension.

Droplet orifices are mounted as shown in Figure 4. The orifices are holes drilled in sapphire blanks and obtained from Flow Industries Inc. They have a re-entrant upstream

configuration as shown by the inset in Figure 4. The orifice mount is designed to hold the orifice blank firmly in place on a flat reference surface. The mount is an integral part of a larger threaded piece which can be removed by hand from the generator to change or clean orifices.

In order to generate a uniform droplet stream a periodic disturbance must be applied to the capillary fluid jet. In the SED 101 this is accomplished by a 5 cm diameter piezoelectric single crystal oscillator mounted in the stand-off shown in Figure 4. The front face of the crystal oscillator is in contact, near the periphery of the crystal face, with an oversized O ring; the rear face is in contact with a teflon backing and is also in contact with a drive lead from a power amplifier (ENI 240L) as illustrated in the figure. The stand-off distance is variable but for all the studies reported here was kept at 2.2 cm.

The operation of the droplet generator is from a control panel with indicator lights and a timer for noting the accumulated length of time that valve No. 1 is open. This is necessary since the diaphragm in the generator has an allowable deflection corresponding to a displacement of about 100 cm³ of liquid.

Filters are incorporated in the system near the orifice and at the inlet to the outgassing reservoir. Despite these precautions some difficulty was experienced with orifice clogging, particularly for diameters below 100 μm .

2.4. Instrumentation

2.4.1. Droplet Visualization

The most useful type of instrument in a first study of any phenomena provides some type of image. The droplets in this study had speeds up to greater than 10^4 cm/s. At this speed a $100\mu\text{m}$ droplet travels its own diameter in about 10^{-6} s. To reduce motion blur of the image to less than one-tenth of a diameter requires an exposure time of 10^{-7} s. For an excellent image a 10^{-8} s exposure time would be more appropriate.

There are a number of approaches to achieving exposure times in the 10^{-7} to 10^{-8} range. For our purposes we decided to use a nitrogen pumped dye laser (Molelectron Spectroscan 10) which was available and was modified to have a 2 mJ, 10^{-8} s pulse. The dye laser pulse was used to expose a closed circuit vidicon camera (Cohu 7120-000). Since the vidicon has about a 30 msec memory and frames at 60 non-interlaced fields per second, there is a sufficiently short time between latent image formation and the next scan for the image to be recorded after it is formed in a 10^{-8} s exposure. The laser was operated between 10 and 20 Hz so that individual exposures could be made and recorded on video tape every three to six fields. A schematic of the imaging system is presented in Figure 5. The components of the system, up to and including the vidicon, are mounted on the optical bench. A reference grid is positioned as indicated, its purpose is to provide a reference marker for judging the frame to frame position of the droplets in the images.

The droplet stream images, which were generally obtained with a nominal magnification of about 20, can be used for a number of purposes. They provide samples of the droplet stream at arbitrary times. These samples, which occur at a rate of between 10 and 20 per second can be used to measure the lateral dispersion of the observed droplets. They can also be used to measure droplet diameters and the

dispersion in longitudinal spacing of the droplets relative to one another. Based on the observation that the droplets close to the generator are evenly spaced, the dispersion in longitudinal spacing measured far from the generator represents a relative speed dispersion of the droplets. The standard deviation of the change in speed of a droplet ($\sigma(\Delta V_d)$) ratioed to the average droplet speed V_d is just,

$$\sigma(\Delta V_d)/(V_d) = \sigma(\Delta t)/\sqrt{2L_F} \quad (3)$$

where Δt is the change in droplet separation and L_F is the length of the flight path. It has been assumed that the individual droplet speed differences are independent, and that the droplets are indistinguishable. Finally, the images give a general visual indication of the configuration of the droplet stream which is valuable information for developing a feel for the parameters that affect droplet stream dynamics.

Because it is time consuming to extract data from these images we have also obtained instruments for direct measurement of stream angular spread or dispersion and droplet speed. A description of these instruments follows.

2.4.2. Direct Measurement of Angular Spread

A schematic of this system appears in Figure 6. A magnified image of the droplet stream is formed parallel to a narrow slit. The image is scanned by the slit in a period of the order of 10^{-1} s using an eight sided mirror rotating at between 1 and 2 rps. The leading edge of the light field in each case triggers a recording device which records the light intensity as the image of the droplet stream is swept by the slit. Since during the time required to traverse the image of about 5×10^{-2} s between 10^3 and 10^4 droplets will be observed, a satisfactory average light attenuation profile can be obtained. The width of one profile will represent the spatial spread of the droplet stream. The repeat profiles are an indication of the steadiness of the stream over long periods (many droplet flight times).

2.4.3. Droplet Velocimeter

This instrument employs the optical train illustrated in Figure 7. Magnified images of the droplet stream are formed perpendicular to a slit aperture which is several stream image diameters long. The instrument is designed to measure absolute speeds of individual droplets and speed dispersion of a continuous droplet stream. Images from the optical access at the top and bottom of the flight tube are superimposed on the slit. The detector is a very fast response photomultiplier tube (EMI 9818B). A single droplet causes a dip in the light flux received by the slit. Thus, for a single droplet the time between two dips in the light level (corresponding to the droplet appearing at the upper and lower optical access ports) gives the droplet flight time, from which speed can be determined. For $100\mu\text{m}$ droplets travelling at 10^4 cm/s a resolution of 1% of the diameter corresponds to 10^{-8}s . Since this is the same order of magnitude as the time required by light to travel 1m, the detector is placed mid-way between the upper and lower access ports. The apparatus is illustrated schematically in Figure 7. The measurement resolution of about 10^{-8}s permits us to determine the flight time of say 10^4 cm/s droplets to an accuracy of better than one part in 10^6 .

The apparatus can also be used to examine the speed dispersion of the stream, or the droplet formation uniformity, by observing the stream continuously using either the lower or upper access ports respectively and measuring the time separation between events. In a manner analogous to the speed dispersion images the time dispersion can be related to speed dispersion by

$$\sigma(\Delta V_d)/V_d = \sigma(\Delta t)/\sqrt{2T_F} \quad (4)$$

where Δt is the time between droplets and T_F the flight time.

3. Nozzle and Stream Fluid Mechanics

3.1. Nozzle Configuration

Traditionally, little attention seems to have been paid to nozzle configuration in droplet generation experiments. For achieving the most coherent droplet stream it is important to consider the fluid mechanics of the stream's nozzle. First of all, since most nozzles are really short tubes, ranging from $L/D = 1$ to $L/D = 10$ (L is tube length, D its diameter) it is important to address the vena contracta (Ref. 5) question. This is done traditionally by forming the entrance to the nozzle or tube with a relatively gradual radius of curvature ($> D/7$).

We have in the present study selected nozzles with an entrance radius of curvature that satisfies this requirement (Figure 4). We have also made a number of calculations of the flows in these nozzles using fairly standard techniques in order to obtain some idea of the flow configurations. The calculations have been made for the two oils in the study, DC-704 and Butyl Phthalate. The properties of these oils are listed in Table I. We have calculated the entrance length in the cylindrical portion of the nozzle before fully developed Poiseuille flow is obtained as well as average stream speed. The entrance length (L_e) is given by (Ref. 5)

$$L_e/D = [\rho V_o / 64\mu] \cdot [3 - K_L] \quad (5)$$

where K_L is a constant equal to 1.3, also μ is the coefficient of viscosity of the fluid and V_o is the average flow speed. The stream speed is obtained by solving the expression for pressure drop across the tube, which for $L \geq L_e$ can be written (Ref. 5) as

$$2\Delta p / \rho V_o^2 = 64L\mu / \rho V_o D^2 + K_L + 1 \quad 6(a)$$

For $L < L_e$ an appropriate expression is

$$2\Delta p/\rho V_0^2 = 64L\mu/\rho V_0 D^2 + (L/L_e)K_L + 1 \quad (6(b))$$

where the (L/L_e) multiplier for K_L is an ad-hoc adjustment for the reduced length over which there is an enhanced shear. The results are shown in Figures 8 and 9. They will be used later in discussing the data obtained in our experiments. Note that if p_s is the stagnation pressure and p_F the flight tube pressure $\Delta p = p_s - p_F \approx p_s$.

3.2. Droplet Formation (U)

Our attention is drawn to capillary jets where surface tension effects dominate gravity. On the ground this means that we refer to liquid streams less than about 1 mm in diameter, in space of course this restriction does not apply, at least for orbiting vehicles. The stability of capillary columns of liquids has been studied for at least a century (Refs. 6,7, 8). In many cases the analysis of moving cylindrical jets of fluid has been treated as being identical to that for stationary columns, the two being related by a simple transformation. It has been pointed out that this is not really correct (Ref. 8) but for our purposes here we will not be overly concerned with the differences. The analyses generally ignore any radial velocity profile in the fluid jet and are for the most part done assuming inviscid fluids. With these simplifications in mind it is found that small axially symmetric disturbances, with a wavelength in the axial direction equal to or greater than the column's circumference, grow and cause the stream to break-up into droplets. Thus

$$\lambda_c = \pi D_0 \quad (7)$$

is the minimum or cut-off wavelength where D_0 is the column diameter, which in general

can be different than the nozzle exit diameter, D. The cut-off frequency for a column flowing axially at speed V_0 is

$$f_c = V_0 / \pi D_0 \quad (8)$$

where f_c is measured at rest relative to V_0 .

The maximum disturbance growth rate given by linear stability analysis occurs at a wavenumber k_o^* of 0.697 where

$$k_o^* = 2\pi/\lambda^*, \lambda^* = \lambda/R_o \quad (9)$$

and $k_o^* = 1.0$ at cut-off. We will use superscript (*) to represent non-dimensional quantities. If a liquid stream is perturbed with a frequency such that the perturbation's non-dimensional wavenumber is between maximum growth and cut-off, the stream is observed to break-up into uniformly spaced, uniformly sized drops (Ref. 9). The minimum break-up time for a column can be written for small initial disturbances (linear theory) and $k_o^* = 0.697$ as

$$t_o = K \{ (\rho R_o^3) / \sigma \}^{1/2} \quad (10)$$

where K is a constant approximately equal to 20. Here, σ is the surface tension and

$$t_c = \{ (\rho R_o^3) / \sigma \}^{1/2} \quad (11)$$

is a characteristic time. For the jet case the break-up time transforms to a break-up distance. The minimum break-up distance for small disturbances is

$$S_o = K V_o \{ (\rho R_o^3) / \sigma \}^{1/2} \quad (12)$$

The various events described above are illustrated schematically in Figure 10. They take place essentially without regard to any gaseous surroundings, at least for pressures of an atmosphere or less and for low stream speeds. Thus, the behavior in a vacuum or in the atmosphere is similar, at least for low speed streams. On the other hand, as we will discuss later, the propagation of the droplets is affected by the atmosphere.

So far, we have ignored viscosity of the fluid. Shown in Figure 11 are the growth rates for an inviscid capillary column and a very viscous capillary column (after Chandrasekhar, Ref. 10) as a function of the wavenumber k_0^* . Note that the cut-off is the same in both cases but for the very viscous fluid there is no preferred frequency and the growth rates are generally smaller. There has been no complete analysis of the effects of viscosity on streams, where the most obvious must be the initial radial velocity profile. The problem has so far defied analytical solution and has only been looked at briefly in one numerical study (see Ref. 8).

The droplet diameter (d) is related through the conservation laws to the stream diameter and the applied disturbance frequency (f) or

$$d = (3/2)^{1/3} \{D_0^2 V_0/f\}^{1/3} \quad (13)$$

Also, the conservation of momentum results in an expression for the droplet speed in terms of the stream speed; where the momentum balance for the control volume shown in Figure 12 for a stream speed V_0 , static pressure in the cylindrical stream of σ/R_0 , and assuming an average over many droplets, gives

$$(\pi D_0^2/4)\rho V_0^2 + (2\sigma/D_0)(\pi D_0^2/4) - \pi D_0 \sigma - (\pi D_0^2/4)V_0 \rho V_d = 0 \quad (14)$$

Here V_d is the droplet speed and the last term of the left hand side of Eqn. (14) is written based on mass conservation. Note that for droplets, the pressure and surface tension forces always cancel at the control surface, from Eqn. (14).

$$V_d = V_o \{1 - \sigma/\rho R_o V_o^2\} = V_o \{1 - V_c^2/2V_o^2\} \quad (15)$$

$$V_c = \{2\sigma/\rho R_o\}^{1/2} \quad (16)$$

Equation (15) is different from the expression obtained in Ref. 11 for V_d where the internal static pressure of the cylindrical stream was neglected. A comparison of the droplet speed data of Ref. (11) to Eqn. (15) is shown in Figure 13.

The droplet separation or pitch is given by

$$l = (V_o/f) (1 - V_c^2/2V_o^2) \quad (17)$$

Generally for water-like surface tension and density $(V_c/V_o)^2 \ll 1$ can be neglected. However for some situations where σ/ρ is an order of magnitude higher (lithium) Eqns. (16) and (17) should be used for droplet speed and spacing.

3.3. Droplet Propagation (U)

3.3.1. Introduction (U)

The major difference between droplet formation from a liquid stream in a vacuum compared to the atmosphere is seen in the droplet stream's propagation. At atmospheric pressure the drops interact with the wakes of previous drops, resulting in a significant angular dispersion and rapid slowing. Ink jet printers, for instance, appear to operate with angular dispersions of the order of milliradians using about 50 μm diameter drops. Without the droplet interactions due to aerodynamics there is no obvious lower limit to the angular dispersion.

The droplet stream that is formed can be a stream of uniformly spaced drops all travelling at closely the same speed. In other situations the droplets can be of various sizes with droplet merging taking place in either a forward or backward direction depending on circumstances, indicating speed differences between the drops. The smaller droplets in the non-uniform case are called satellites. A schematic description of satellite formation and merging terminology is given in Figure 14. If the satellites merge with their parents then the stream ends up with uniformly sized drops moving at nearly the same speed. If, as sometime happens, the satellites merge with drops other than their parents the result may be rapid drop growth and possibly stream disruption. These effects have not yet been studied in detail over long flight paths.

It has been noted by Chaudhary (Ref. 9) based on his non-linear analysis that no satellites appear for pure fundamental wave numbers greater than 0.65. However, experiments by Pimbley and Lee (Ref. 12) indicate that satellites do appear at all wave numbers. Chaudhary also finds experimentally that for each k_0^* there is a transition from forward separation to rearward as the disturbance amplitude is increased. Chaudhary found experimentally that as the disturbance amplitude is increased, the satellites change from rear-merging to forward merging. This is in general agreement with Pimbley and Lee who noted that the merging takes place in the direction of the last attached point of the satellite, which implies that merging is in the opposite same to separation. However, this does not appear to be a strict rule as indicated by Chaudhary. Chaudhary also demonstrated both theoretically and experimentally that the input of harmonics of the fundamental disturbance frequency can be used to affect satellite formation and merging. The non-linear analyses by Chaudhary (Ref. 9) and others (Ref. 8) have also shown that the cut-off wave number becomes an increasingly wide cut-off zone with increasing disturbance amplitude. There are other detailed changes that we will not discuss here.

3.3.2. Estimate of the Order of Magnitude of Droplet Velocity Perturbations

It is of interest to estimate the order of magnitude of possible droplet velocity perturbations. This is attempted in the following. Consider the fluid flow speed induced in a capillary stream by motion of the stream surface. A sketch of typical flow streamlines in a liquid column is shown in Figure 15. The surface motion will be assumed to be a pure harmonic function with the amplitude growth matched to calculated break-up times from the non-linear analysis of Chaudhary (Ref. 9). For the coordinate system and nomenclature shown in Figure 15, we want to calculate the perturbation momentum and from this the drop velocity perturbation for the fluid to the right of $Z = Z_B$ up to $Z = \lambda/2$. The location Z_B is a hypothetical break position. It is assumed that there are no satellites and the mechanism for velocity perturbations is small variations in the position of drop separation, which in this case is modelled by the break position Z_B .

The surface profile is given by

$$r'(Z,t) = R_0 \epsilon^* e^{t/K't_c} \cos(2\pi Z/\lambda) \quad (18)$$

and the maximum displacement

$$r'_m = \epsilon^* R_0 e^{t/K't_c} \quad (19)$$

where ϵ^* is the amplitude of the initial disturbance, $\epsilon^* = r'_m / R_0$.

By calculating the time rate of change of volume of the stream between $Z = Z^1$ and $\lambda/2$, and applying conservation of mass, the average Z direction flow speed at Z^1 for the incompressible fluid is

$$u(Z^1,t) = 2\pi \frac{\int_{Z^1}^{\lambda/2} r(Z,t)(dr(Z,t)/dt)dZ}{\pi \{r(Z^1,t)\}^2} \quad (20)$$

where $r(Z,t) = R_0 + r'(Z,t)$.

The total perturbation momentum associated with the $u(Z^1, t)$ between $Z^1 = Z_B$ and $Z^1 = \lambda/2$ is

$$\Delta P_d(Z_B, t) = \rho \pi \int_{Z_B}^{\lambda/2} u(Z^1, t) r(Z^1, t)^2 dZ^1 \quad (21)$$

For a droplet momentum of P_d and assuming $V_d = V_o$:

$$\Delta P_d(Z_B, t)/P_d = 3 \int_{Z_B}^{\lambda/2} u(Z^1, t) [r(Z^1, t)]^2 dZ^1 / 4R_o^3 V_o \quad (22)$$

Since we are only interested in the perturbation momentum at break-up the $\epsilon^* e^{t/K^1 t_c} = 1$ by definition when $t = T_b$, the break-up time. Applying this to Eqn. (22) removes time as a variable and Eqn. (27) reduces to

$$\Delta P_d(Z_B/\lambda)/P_d = \{6\pi^2 \sigma^{1/2} / k_o^{*2} R_o^{1/2} V_o K^1 \rho^{1/2}\} \Gamma(Z_B/\lambda) \quad (23)$$

Taking the change of mass of a droplet into account it can be shown that the order of magnitude of a droplet velocity change ΔV_d corresponding to a break-up at Z_B is

$$\Delta V_d/V_d = \Delta P_d/P_d \quad (24)$$

The fractional mass change of the droplet is

$$\Delta M_d/M_d = \int_{Z_B}^{\lambda/2} \pi R_o^2 (1 + \cos(2\pi Z/\lambda))^2 dZ / \int_{-\lambda/2}^{\lambda/2} \pi R_o^2 (1 + \cos(2\pi Z/\lambda))^2 dZ \quad (25)$$

We have evaluated $\Gamma(Z_B/\lambda)$ and $\Delta M_d(Z_B/\lambda)/M_d$, they are shown in Figure 16. We will use these values later in this report to estimate velocity perturbations from Eqn. (24) for our experimental conditions.

3.3.3. External Forces on the Stream at the Nozzle Exit

As will be discussed later there is experimental evidence which suggests that the stream wanders perpendicular to the axis prior to its break-up into droplets. We consider here a model of the nozzle exit flow as illustrated in Figure 17. A force analysis on the stream as an isolated body, using Newtons laws, yields

$$F_x = (\pi D_0^2/4) \rho V_0^2 d\theta \quad (26)$$

assuming the stream has an average speed V_0 and $d\theta$ is the angular deviation of the stream. Similarly, in the axial direction

$$F_z = (\pi D_0^2/4) \rho V_0^2 (dV/V_0) \quad (27)$$

where dV is the axial speed deviation of the stream.

In the experiments $d\theta$ and dV are measured, they can be related to F_x and F_z using equations (26) and (27).

3.3.4. Relationship Between Stream Radius Perturbation and Stagnation Pressure Changes

It is of interest to develop a feeling for the relationship between stagnation pressure fluctuations caused by the piezoelectric crystal and the resulting induced stream radius changes. Assume a small periodic pressure perturbation in the stagnation chamber of $p'(t)$ with a maximum amplitude p'_m . If the incremental mass flow associated with the $p'(t)$ is immediately converted to a stream radius perturbation r' the disturbance amplitude can be written as $\epsilon^* = r'_m/R_0$, or $\epsilon^* = 2V'_m/V_0$ where V'_m is the stream axial velocity perturbation at the nozzle exit. Using Bernoulli's equation

$$V'(t)/V_0 = p'(t)/2p_s \quad \epsilon^* = p_m/p_s \quad (28)$$

The power required to apply the pressure oscillations can be found as

$$P_R = (Mp'_m/\rho) [1 - p_s/\rho a^2] \quad (29)$$

where a is the sound speed in the fluid and M is the mass of fluid that is involved.

3.4. Droplet Impact on Liquid and Dry Surfaces (U)

The impact of small droplets of non-wetting liquids with moderate surface tensions on dry surfaces is not directly affected by gravity. The drop will spread over the surface due to its momentum, with the spread resisted by surface tension forces. The ratio of the maximum spread diameter to the original droplet diameter is called a spread factor F , from (Ref. 13)

$$F = 0.82 (W^*)^{1/4} \quad (30)$$

where W^* is the Weber number,

$$W^* = V_0^2 d / \sigma \quad (31)$$

After impact the droplet spreads to a maximum diameter and then oscillates about a final equilibrium position that depends on the surface tension of the materials. The ratio of the stationary diameter (D_s) to the original droplet diameter is (Ref. 13)

$$D_s/d = \{4\sin^3 \theta_c / (2 - 3\cos \theta_c \cos^3 \theta_c)\}^{1/3} \quad (32)$$

where θ_c is the contact angle given by

$$\sigma_s - \sigma_{LS} = \sigma_L \cos \theta_c \quad (33)$$

If the surface is wet the $\sigma_{LS} = 0$ and $\sigma = \sigma_L$ so that $\theta_c = 0$ and a drops spreads over the entire surface area. If the surface is dry, the value of D_s depends on the surface tension

of the three interfaces involved, liquid (L), liquid-solid (LS) and solid (S). The contact angle θ_c is the angle determined by the liquid-solid interface and the tangent to the free liquid surface at the contact point between liquid and solid. In many cases the dynamic spread will be considerably larger than the static spread.

If the Weber number approaches large values (10^4) the drops may be expected to shatter as they impact the surface. The shatter may not be entirely a bounce but simply spread small discrete quantities of material over a large surface area. The impact characteristics may also be affected by the viscosity of the drops. As a measure of the relative importance of viscous effects to surface tension the capillary number (C^*) is used. If the surface is a pool of fluid there will generally be fluid ejected from the surface in a gravitational field (Refs. 13 and 14). The behavior at zero gravity may be quite different and remains to be investigated.

4. Results (U)

We have done a number of experiments, observing both droplet formation and the results of the subsequent droplet dynamics for low vapor pressure fluids injected into a high vacuum. The majority of the data is recorded as images on video tape. We have done experiments on measuring low vapor pressure oil conductivity, droplet charging and deflection. The interaction of streams of high Weber number droplets with an aluminum surface in a vacuum has been observed. In all the experiments for which data is reported the indicated power from the power amplifier was 200w. No effort was made to determine the amount of power coupled into the liquid although it appeared to be a small fraction of 200w.

4.1. Average Stream Speeds

Since it is essential to know the stream speed in order to interpret our results we took the time to make some speed measurements. Using DC-704 and the 183 μm diameter orifice, we predicted average fluid speeds as a function of stagnation pressure using Eqns. 5 and 6 and compared these to experimental average speeds obtained from volume flow measurements. The results are shown in Figure 8 and are seen to be in excellent agreement with the prediction. The length of the cylindrical portion of the orifice (see Figure 4) was measured using a binocular microscope and found to be close to 400 μm , this value was used in the predictions. It is interesting to note that for the majority of cases considered, the entrance length (Eqn. 5) is larger than the tube length as indicated by the calculated results in Figure 9. Consequently the average speed predictions are based on Eqn. 6b, which is an ad hoc construct that we have developed for the purposes of this investigation.

Since the average speed prediction technique appears quite accurate, we have used calculated speeds in specifying parameters at which we operated in any particular experiment.

4.2. Angular and Speed Dispersions (U)

As described in Section II.4.a we have used the video records to measure the angular and speed dispersion of various droplet streams. The general configurations that have been attempted are outlined in Table II. The high viscosity oil, DC 200, did not give a successful droplet stream although this was only one try and should be repeated if high viscosity fluids are attractive for particular applications. The small orifice became plugged several times when we were attempting to do experiments because of excessively dirty oil. Due to time constraints we were unable to correct this problem and

do a series of meaningful experiments with this orifice. The large orifice permitted the Butyl Phthalate to drain from the stagnation chamber. This in turn caused all sorts of havoc when the No. 1 valve was opened, the high pressure causing the liquid to flow violently into the stagnation chamber. The re-filling of the stagnation chamber used up most of the available diaphragm deflection so that we were unable to obtain meaningful data for the 183 μ m orifice using Butyl Phthalate.

For the other configurations outlined in Table II there are some general observations that seemed to be common enough to be worth mentioning. These are listed below in point form, but in no particularly significant order.

- * There were noticeable effects on the droplet spacing uniformity by going from say 10⁻² torr to 10⁻⁴ torr in flight tube pressure.
- * The droplet stream position was stagnation pressure dependent, changing its position at the end of the flight tube by a few centimeters over the stagnation pressure range from say 150 to 1500 psi. This was likely due to deflection of the orifice mounting structure.
- * The data indicates that it was necessary to outgas the liquid to pressures < 10⁻⁴ torr to obtain the most coherent droplet streams.
- * There was a starting time evident in many of the runs which could not be readily explained based on the experimental parameters; although each test configuration seems to have its own characteristic time.
- * In some cases the starting transient was around a second which is the time required for valve No. 1 to open, in other cases the droplet stream seemed to jump back and forth plus or minus 10 μ rad or so and then, after perhaps 5 seconds, settle down to an order of magnitude less angular jitter.
- * While the droplet stream orientation clearly depends on the orifice orientation, once established the stream was very repeatable. This is evident because we were able to work with a very small field of view (\pm 2.5 mm) for the imaging system.
- * Examination of the video frames leaves the impression of occasional catastrophic upsets in stream droplet spacing accompanied by exceptionally large droplets. Some of the configurations were more susceptible to this than others.

These observations are to be read with the general caveat that they are derived from impressions obtained as a result of studying the video tape results. The taped results are arbitrary samples (not random necessarily) of the phenomena. Much more data, using rigorous statistical sampling techniques (e.g. random number generators to trigger the dye laser) would have to be obtained and reduced quantitatively before the caveats could be removed. This is well beyond the scope of the present study. It appeared important however, to record our impressions in order to help guide the direction of future investigations. Besides, we really do not expect that rigorous sampling techniques would significantly alter the observations that we have made.

We have obtained quantitative data from the video tapes. The magnifications of the video images are known by calibration. By direct measurement of distances on the video display we are able to obtain measures of the angular dispersion of the droplets and relative speed dispersions as discussed before. The questions about the nature of the sampling process remain, but at this initial stage of investigation these are certainly of minor importance.

A measure of the speed dispersion is obtained by determining the separation (Δl) between consecutive droplets in any particular image (usually 5-10 droplets per image). A mean separation is calculated for each image in a particular run (a time duration of about 0.3s or around twenty images per run) and from the mean results for each image a mean separation obtained for the run. A run consists of operation at a given stagnation pressure with a particular liquid, oscillator frequency and orifice. Using the mean, standard deviations in the separation are calculated for each frame and for the complete run. The angular dispersion or dispersion in lateral displacement of the stream is found somewhat differently. It is observed that in each frame the droplets lie on a straight line. The lateral displacement was determined by measuring the displacement perpendicular to

the stream (from a fixed point on the reference grid), of a line passed through the droplet centers. Thus each image represents one lateral displacement or the average displacement of all the droplets in that image. A mean displacement which is meaningless due to the arbitrary zero, and standard deviation are determined for the run from approximately 20 images.

Some judgment has been applied to the selection of the frames to be used in a given run. It was observed that there appeared to be a starting transient that lasted for varying lengths of time, depending on the test configurations. The data we have selected for analysis is in our judgment after this starting transient. Clearly, there could be some discussion of what is transient and what is not; so there is some possibility for opinion to enter the quantitative data because of this. In all cases, once the starting transient was judged to have been completed, approximately 20 consecutive video images were analyzed.

The results of our analysis of a number of experimental runs are listed in Appendix I. These are in terms of video display screen dimensions in centimeters. The angular results are actually lateral displacements so that the flight path length of 540 cm must be used to turn them into an angle, as well as the magnification.

The speed and angular dispersion results are tabulated in Table III for the two fluids and orifice diameters, along with other parameters appropriate to each experiment.

Notice in Table III that the higher reservoir pressure is associated with an order of magnitude greater angular scatter but not a big difference in axial speed dispersion. Using Eqn. (26) gives a force $F_1 = 13 \times 10^{-2}$ dynes for $d\theta = 20 \times 10^{-6}$. If the model of the exit surface wetting shown in Figure (17) is adopted, the only possibility for reaching this order of magnitude of F_1 is for the gas to boil and tear the surface of the fluid in the

region away from the stream on the nozzle's exit surface, where the liquid layer has little curvature and hence the internal pressure is low. If half the perimeter of the liquid surface is torn a net force of around 70×10^{-2} dynes would be generated. Some mechanism like this is plausible since the stream appears to move prior to break-up; in each frame all the droplets tend to lie on the same flight path. There is little possibility that pressure due to the dissolved gas evaporating from the stream could cause the observed angular deviation. An imaginary bubble with $50 \mu\text{Hg}$ internal pressure applied over an area D_0^2 perpendicular to the stream results in a force of only $F_z \approx 2 \times 10^{-2}$ dynes.

For the Z direction speed dispersion, tearing of the surface may be part of the cause of the observed deviation since the surface tension in this direction corresponds to around 300×10^{-2} dynes for the entire periphery of the stream's liquid column. However, a mechanism for tearing in the relatively highly curved surface surrounding the stream is not obvious. Also, there is a relatively large residual speed dispersion (corresponding to $F_z \approx 10 \times 10^{-2}$ dynes) at low reservoir pressures. In addition, the droplet speed dispersion applies to individual droplets, unlike the angular dispersion. Another source of the speed dispersion is the perturbation momentum discussed above in Section III-3.b. Using the results in Figure 16 and Eqn. (24) we estimate a speed dispersion of 100×10^{-6} for a break-up variation corresponding to 3×10^{-4} variation in droplet mass. It is thus quite plausible that the droplets develop significant speed variation as a result of very small irregularities in the break-up process.

4.3. Stream Charging

The charging of liquid droplets can be used to direct a droplet stream, as in ink jet printing. It is of interest to be able to control the direction of droplet streams in a vacuum. The simplest such control can be achieved by electrostatic deflection. As a result we have investigated the possibility of obtaining appropriate conductivities in the very insulating vacuum oils by using a charge control additive.

Charging of a stream of droplets has been discussed by Schneider et al (Ref. 11). A charging electrode is used to apply an electric field to the liquid stream prior to break-up. A conducting liquid such as water (2×10^{-4} mhos/m) is required so that a current flows in the liquid in an attempt to neutralize the superimposed field. The stream is caused to break-up in a region within the charging electrode. When the stream breaks-up into droplets, residual net charge remains with each droplet. The drops can be deflected by applying transverse electric fields or magnetic fields as in electron or ion guns. If the stream liquid is not conducting, then either some active form of stream charging is required or a solute that is ionized in solution must be added.

We have measured the conductivity of DC-704 and Butyl Phthalate in a conductivity cell¹. The results are shown in Figure 18. Also shown in the figure are conductivities that are obtained by adding small amounts of zirconium octoate to the oils. This additive is used in certain liquid toners in the copying industry as a charge control agent. Note that the DC-704 is a very poor conductor, even when the additive is used. The Butyl Phthalate is a better conductor getting reasonably close to water when the additive is used. In our droplet charging experiments we have used the Butyl Phthalate. The charging electrode arrangement is indicated in Figure 19. In our first experiments we

¹This work done by R. Duenas

measured the current to a droplet receiver for various potentials applied to the charging electrode. Using unaltered Butyl Phthalate, 200 psig, $D = 146 \mu\text{m}$, we observed 3×10^{-10} amp current independent of applied potential to the charging electrode. The observed current corresponds to about 4×10^4 charges per drop. Using the results of Schneider et al (Ref. 11), 4×10^7 charges per drop would be expected for a sufficiently conducting fluid. The charge that is observed is independent of potential and is of a magnitude that is expected due to contact potentials. We have not yet had an opportunity to try the more conducting Butyl Phthalate with added zirconium octoate.

4.4. Droplet Impact Experiments (U)

Droplet streams have been directed on to an aluminum plate at an incident angle of 45° from the outward normal. A summary of the stream conditions is in Table IV and V. The g vector was in the same direction as the droplet stream. A schematic of the experimental set-up is shown in Figure 20.

In each case the results were similar, although different in degree. The impact caused the generation of very small droplets (about 1/50 of the parent size) due to shattering. The shattered drops were noticed primarily because the windows to the test area acted as witness plates. In the stream with the DC-704 the windows were degraded for purposes of laser imaging after about 5 to 10 seconds. For the Butyl Phthalate streams the windows became opaque in only a few frames of the imaging system. For the DC-704 stream an obvious large majority (90%) of the liquid remained in contact with the plate whereas for the Butyl Phthalate the amount was much less (say 20-25%). These capture percentages are only very approximate and were made by visual observation of the events.

In both cases the flow field is represented by the sketch in Figure 21. It is

interesting to notice in Table V that some combination of the Capillary number and Weber number is needed to describe the impact shattering. The more viscous DC-704 does not shatter nearly as much as the Butyl Phthalate despite similar W^* .

For the DC-704 stream some successful video images of the impact were obtained. From these images it is evident that the collision of a droplet stream with a surface is complicated. Droplets tend not only to collide with the surface, but with the preceding droplet as it is slowed during the collision process. Thus the impact of typical streams with closely spaced droplets is really some combination of drop-surface and droplet-droplet collisions.

5. Conclusions

While the results obtained in this study must be verified in further experiments, it is possible to formulate a useful set of conclusions.

- * Angular root mean square spreads of less than 1 μrad have been obtained for droplet streams travelling at 24 and 121 m/s with droplet diameters of 280 and 240 μm respectively.
- * The average root mean square angular spread for droplet streams using well outgassed liquid was around $\pm 2 \mu\text{rad}$.
- * The average root mean square stream-wise droplet velocity variation for the streams of well outgassed liquid was $\pm 16 \times 10^{-6}$
- * Using liquid saturated with air at 50 μHg pressure resulted in significantly greater angular dispersion and somewhat greater stream-wise velocity dispersion. However, this was also with a 30% larger stream nozzle diameter.
- * The stream-wise velocity dispersion appears to be very sensitive to the applied frequency and thus also to the stream speed. Neither of these parameters were controlled with great precision (probably to about $\pm 0.2\%$). Much more precise control over these parameters may be necessary to reduce the velocity dispersion significantly.
- * Comparing two cases, one having just achieved fully developed pipe flow in

the nozzle, the other having a relatively very small boundary layer, indicates that there is no noticeable effect on the angular dispersion. The fully developed pipe flow case exhibits a greater stream-wise velocity dispersion, but not outside the general variation of the results for other streams.

- * A simplified analysis indicates that the stream-wise velocity dispersion of the droplets may be due to small variations in the break-off points of the droplets.
- * The angular dispersion is not in general a drop to drop dispersion but appears to originate from a disturbance applied to the stream before break-up. A candidate is variation of radially directed surface tension forces resulting from the rupture of a liquid surface layer that has wet the exit surface of the nozzle.
- * Droplet impact experiments at 45° angle of incidence to a flat plate indicate that approximately $250\mu\text{m}$ diameter droplets shattering at high Weber number (6×10^4) are sensitive to a fluid viscosity change from 14 to 37 centistokes. The higher viscosity fluid scattered significantly less material away from the surface.
- * Butyl Phthalate (a vacuum oil of modest vapor pressure) can be made to have a conductivity of about two orders of magnitude less than water by adding about 0.3% by volume of zirconium octoate.
- * For unaltered Butyl Phthalate we observe about 4×10^4 charges per drop independent of charging electrode voltage up to 1000 V.
- * For a sufficiently conducting fluid we would expect around 5×10^7 charges per drop. Further work needs to be done with the zirconium octoate added to the liquid.
- * Charge control on the droplets is of interest because it offers a means for controlling stream direction. On the other hand, highly charged droplets in multiple streams may cause an unacceptable blooming of the droplet array.
- * The Droplet Dynamics Space Simulator and the other instruments designed for this study work very well.
- * For further studies a mechanical alignment device for the droplet stream would be useful. Although, the original concern (and reason for not installing such a device in the first place) that it might introduce a certain amount of stream directional dispersion still needs to be carefully thought through.
- * One area of research that has not been addressed here in any detail, but which may be important for applications, is where the stream speed (V_o) and characteristic speed (V_c) are of the same magnitude. In this case there is evidence in the theoretical literature that there is an increased regime of unstable wave numbers.

Acknowledgements

The Authors would like to thank D. Kingsbury and C. de Vries for their valuable advice expert assistance along with Mark Trojanowski for his contributions. The work was supported by the Air Force Rocket Propulsion Laboratory under contract number RPL F04611-82-K-0040.

References

- (1) A.T. Mattick and A. Hertzberg. The liquid droplet radiator - ultra lightweight heat rejection system for efficient energy conversion in space. *Acta Astronautica*, 9, 3, 165-172, 1982.
- (2) E.P. Muntz, S-S. Qian, M. Dixon, The injection of fluids into vacuum: applications to space and rarefied gas dynamics, to be presented, 14th International Symposium on Rarefied Gas Dynamics, Tsukuba, Japan, 1984.
- (3) J.M. Schneider, N.R. Lindblad, C.D. Hendricks. An apparatus to study the collision and coalescence of liquid aerosols, *J. Colloid Sci.*, 20, 610-616, 1965.
- (4) Newport Corporation, Catalog, 1982.
- (5) J.A. Owczarek, Introduction to Fluid Mechanics, International Textbook Co., Scranton, 1968.
- (6) Lord Rayleigh, On the instability of jets, *Proc. Lond Math. Soc.*, 10, 4, 1878.
- (7) A. Lawley, Atomization of specialty powders, *J. of Metals*, 13-18, January 1981.
- (8) D.R. Bogy, Drop formation in a circular liquid jet. *Ann. Rev. Fluid Mech.* 11, 207, 1979.
- (9) K.C. Chaudhary, The nonlinear capillary instability of a jet, Ph.D. dissertation, University of Southern California, 1977.
- (10) S. Chandrasekhar, Hydrodynamic and Hydromagnetic Stability, Ch. X11, Oxford at the Clarendon Press, 1961.
- (11) J.M. Schneider, N.R. Lindblad, C.D. Hendricks, J.M. Crowley, Stability of an electrified liquid jet, *J. Appl. Phys.*, 38, 6, 2599-2605, 1967.
- (12) W.T. Pimbley, H.C. Lee, Satellite droplet formation in a liquid jet. *IBM J. Res. Dev.*, 21, 21, 1977.
- (13) L. Cheng, Dynamic Spreading of drops impacting onto a solid surface, *Ind. Eng. Chem. Process Des. Dev.*, 16, 2, 192-197, 1977.
- (14) F.H. Harlow, J.P. Shannon, The splash of a liquid drop, *J. Appl. Phys.*, 38, 10, 3855-3866, 1967.
- (15) F.H. Harlow, J.P. Shannon, Distortion of a splashing liquid drop, 157, 547-550, August, 1967.

TABLE I
PROPERTIES OF LIQUIDS USED IN EXPERIMENTS*

Liquid	Kinematic Viscosity centistokes	Surface Tension dynes/cm	Density gm/cm ³	Vapor Pressure torr
DC 704	39	37	1.07	9×10^{-8}
Butyl Phthalate	14.4	50	1.04	1×10^{-4}
DC 200	100	-	1.0	10^{-4}

*At 28°C

TABLE II
COMMENTS ON TEST CONFIGURATIONS

Orifice Diameter (μm)	DC 704	Butyl Phthalate	DC 200
146	Results for a range of p_s and f	Results for a range of p_s and f	Did not attempt
183	Results for a range of p_s and f	Liquid not retained in stagnation chamber	Unsuccessful
76	No data obtained	Did not attempt	Did not attempt

TABLE III

Liquid	D (μm)	P_s (psi)	f (kHz)	v_o (m/s)	k_o^*	$\lambda = v_o/f$ (cm)	λ_{OBS} (cm)	$d = \left\{ \frac{3}{2} D^2 \lambda_{OBS} \right\}^{1/3}$ (μm)	$\sigma(v_d) \times 10^6$ $\frac{v_d}{V_d}$	$\sigma(\theta) \times 10^6$ (radians)	Comments
704	183	147	28	27	.67	0.10	0.10	365	33	36	Liquid outgassed
704	183	511	58	58	.56	0.10	0.10	370	29	22	to $50\mu\text{H}_g$
704	183	995	84	100	.52	0.11	0.12	390	37	11	in reservoir
704	146	204	33	24	.59	.07	.07	280	21	<1	Liquid outgassed
704	146	506	66	49	.59	.07	.06	270	13	3	to $\leq 10^{-4}$ torr
704	146	1410	132	100	.59	.07	.06	260	11	2	in reservoir
B.P.	146	198	59	38	.74	.06(5)	.05	250	12	3	Liquid outgassed
B.P.	146	500	103	67	.71	.06(5)	.05	250	25	2	to $\leq 10^{-4}$ torr
B.P.	146	1408	185	121	.69	.06(5)	.04	240	12	<1	in reservoir

TABLE IV
SURFACE IMPACT EXPERIMENTS

P_s (psi)	D (μm)	DC 704	Butyl Phthalate
1000	146	Video window fogging noticeable after 5s.	-
1300	146	-	Video, severe window fogging in 1/2s.
200	146	-	Real time visual observation, moderate to severe fogging 1/2s.

TABLE V
SURFACE IMPACT EXPERIMENTS

P_s (psi)	Liquid	d (cm)	v_d (cm/s)	W^*	Re_d^*	$\frac{W^*}{Re_d^*}$	Window Fogging or bounce
1000	DC 704	0.026	0.84×10^4	5.3×10^4	5.6×10^2	95	Light
200	Butyl Phthalate	0.025	0.38×10^4	0.73×10^4	6.3×10^2	12	Moderate to severe
1300	Butyl Phthalate	0.024	1.16×10^4	6.9×10^4	19×10^2	36	Severe

APPENDIX I
DATA

DC 704 182.88 MICRONS, 1000 PSI

FRAME	MEAN	STANDARD DEVIATION
1	1.633	0.125
2	4.500	0.000
3	3.550	0.350
4	2.950	0.850
5	2.000	0.900
6	2.433	0.660
7	1.867	0.492
8	3.350	0.150
9	1.600	1.000
10	3.150	0.350
11	2.350	0.150
12	1.567	0.556
13	2.800	0.000
14	1.600	1.678
15	2.500	1.000
16	4.300	0.000
17	2.700	0.000
18	1.725	0.449
19	3.300	0.000
20	1.767	0.205
21	1.267	0.330
22	3.800	0.000
23	1.767	1.228
24	1.675	0.286
25	2.067	0.419

Mean of run is 2.488667

Mean deviation of spacing in run is 0.8594828.

Standard deviation of run is 0.8002873.

Mean angular deviation of run is 9.7280018E-02.

Standard angular deviation is 0.1170299.

APPENDIX I
DATA

DC 704 182.88 MICRONS 500 PSI

FRAME	MEAN	STANDARD DEVIATION
1	1.650	0.844
2	2.000	0.212
3	2.500	0.300
4	1.875	0.370
5	2.033	0.330
6	1.800	0.082
7	1.900	0.294
8	1.800	0.430
9	1.833	0.262
10	1.800	0.356
11	1.933	0.189
12	2.500	0.000
13	2.067	0.660
14	1.900	0.173
15	2.033	0.613
16	1.667	0.386
17	2.000	0.200
18	1.925	0.327
19	2.067	0.189
20	2.033	0.660
21	1.800	0.500
22	1.667	0.858
23	2.000	0.000
24	1.833	0.236
25	2.800	0.000

Mean of run is 1.976667

Mean deviation of spacing in run is 0.6680000.

Standard deviation of run is 0.6176389.

Mean angular deviation of run is 0.1516801.

Standard angular deviation is 0.2506312.

APPENDIX I
DATA

DC 704 146.3 MICRONS 200 PSI

FRAME	MEAN	STANDARD DEVIATION
1	1.475	0.083
2	1.625	0.130
3	1.525	0.043
4	1.750	0.087
5	2.000	0.283
6	2.100	1.417
7	1.500	0.000
8	1.360	0.388
9	1.525	0.043
10	1.660	0.488
11	1.500	0.000
12	1.533	0.047
13	1.525	0.327
14	1.500	0.543
15	1.500	0.458
16	1.425	0.492
17	1.433	0.170
18	1.500	0.000
19	1.420	0.194
20	1.525	0.043

Mean of run is 1.569083

Mean deviation of spacing in run is 0.4602111.

Standard deviation of run is 0.5021021.

Mean angular deviation of run is 2.9802322E-08.

Standard angular deviation is 2.9802322E-08.

APPENDIX I
DATA

B.P. 146 MICRONS 1408 PSI

FRAME	MEAN	STANDARD DEVIATION
1	1.083	0.186
2	1.080	0.117
3	1.080	0.098
4	1.050	0.214
5	1.083	0.121
6	1.060	0.250
7	1.000	0.126
8	1.000	0.179
9	1.040	0.150
10	1.080	0.098
11	1.000	0.297
12	0.980	0.256
13	1.300	0.412
14	1.080	0.098
15	1.060	0.136
16	1.080	0.075
17	1.120	0.160
18	0.940	0.215
19	1.040	0.080
20	1.020	0.098
21	1.000	0.000
22	1.020	0.133
23	1.080	0.214
24	1.060	0.049
25	1.080	0.075

Mean of run is 1.056667

Mean deviation of spacing in run is 0.4127822.

Standard deviation of run is 0.3192367.

Mean angular deviation of run is 0.0000000.

Standard angular deviation is 0.0000000.

APPENDIX I
DATA

DC 704 188 MICRONS, 150 PSI

FRAME	MEAN	STANDARD DEVIATION
1	1.700	0.100
2	1.750	0.050
3	1.800	0.163
4	1.900	0.596
5	1.833	0.047
6	1.850	0.087
7	1.900	0.500
8	2.033	0.047
9	2.250	0.250
10	2.133	0.330
11	2.033	0.249
12	2.033	0.047
13	2.033	0.236
14	1.833	0.759
15	1.867	0.094
16	1.000	0.000
17	2.067	0.368
18	2.400	0.849
19	2.000	0.589
20	1.950	0.050
21	2.233	0.189
22	2.350	0.850
23	1.967	0.262
24	1.825	1.143
25	1.800	0.589

Mean of run is 1.941667

Mean deviation of spacing in run is 0.6685714.

Standard deviation of run is 0.7170666.

Mean angular deviation of run is 0.3232000.

Standard angular deviation is 0.3931209.

APPENDIX I
DATA

DC 704 146 MICRONS, 1400 PSI

FRAME	MEAN	STANDARD DEVIATION
1	1.250	0.150
2	1.340	0.049
3	1.260	0.049
4	1.240	0.049
5	1.260	0.049
6	1.260	0.080
7	1.220	0.117
8	1.200	0.000
9	1.300	0.110
10	1.425	0.576
11	1.280	0.040
12	1.225	0.043
13	1.300	0.000
14	1.440	0.314
15	1.220	0.117
16	1.200	0.141
17	1.320	0.098
18	1.283	0.107
19	1.300	0.190
20	1.100	0.126
21	1.267	0.125
22	1.300	0.190
23	1.220	0.160
24	1.300	0.000
25	1.260	0.162

Mean of run is 1.270800

Mean deviation of spacing in run is 0.2960656.

Standard deviation of run is 0.2721901.

Mean angular deviation of run is 2.1120001E-02.

Standard angular deviation is 3.2496154E-02.

APPENDIX I
DATA

DC 704 146 MICRONS, 500 PSI

FRAME	MEAN	STANDARD DEVIATION
1	1.420	0.075
2	1.467	0.075
3	1.460	0.150
4	1.480	0.098
5	1.380	0.098
6	1.500	0.219
7	1.460	0.196
8	1.460	0.080
9	1.483	0.107
10	1.440	0.049
11	1.300	0.167
12	1.480	0.183
13	1.500	0.063
14	1.400	0.100
15	1.480	0.417
16	1.480	0.098
17	1.420	0.098
18	1.520	0.264
19	1.480	0.040
20	1.380	0.075
21	1.400	0.089
22	1.480	0.098
23	1.420	0.098
24	1.450	0.369
25	1.480	0.040

Mean of run is 1.448800

Mean deviation of spacing in run is 0.3749355.

Standard deviation of run is 0.3190061.

Mean angular deviation of run is 3.1999998E-02.

Standard angular deviation is 3.9999999E-02.

APPENDIX I
DATA

B.P. 146 MICRONS, 500, OPSI

FRAME	MEAN	STANDARD DEVIATION
1	1.180	0.223
2	1.125	0.043
3	1.125	0.432
4	1.150	0.206
5	1.567	0.380
6	1.050	0.415
7	1.175	0.249
8	1.275	0.148
9	0.975	0.249
10	1.125	0.083
11	0.975	0.249
12	1.200	0.604
13	2.125	1.746
14	1.133	0.236
15	0.867	0.189
16	1.300	0.900
17	1.150	0.087
18	1.050	0.087
19	1.067	0.189
20	1.175	0.487
21	1.075	0.455
22	1.100	0.406
23	1.100	0.100
24	1.000	0.424
25	1.300	0.367

Mean of run is 1.174533

Mean deviation of spacing in run is 0.7335815.

Standard deviation of run is 0.6842672.

Mean angular deviation of run is 2.399998E-02.

Standard angular deviation is 2.4494901E-02.

APPENDIX I
DATA

B.P. 146 MICRONS, 198 PSI

FRAME	MEAN	STANDARD DEVIATION
1	0.660	0.540
2	1.220	0.040
3	1.200	0.071
4	1.175	0.179
5	1.375	0.377
6	1.225	0.043
7	1.175	0.249
8	1.200	0.000
9	1.250	0.320
10	1.200	0.000
11	1.500	0.589
12	1.175	0.205
13	1.200	0.000
14	1.200	0.000
15	1.200	0.000
16	1.200	0.000
17	1.475	0.334
18	1.225	0.043
19	1.200	0.000
20	1.250	0.180
21	1.225	0.043
22	1.200	0.000
23	1.200	0.000
24	1.200	0.089
25	1.225	0.043

Mean of run is 1.214200.

Mean deviation of spacing in run is 0.2884654.

Standard deviation of run is 0.3202142.

Mean angular deviation of run is 8.3200023E-02.

Standard angular deviation is 0.03666.

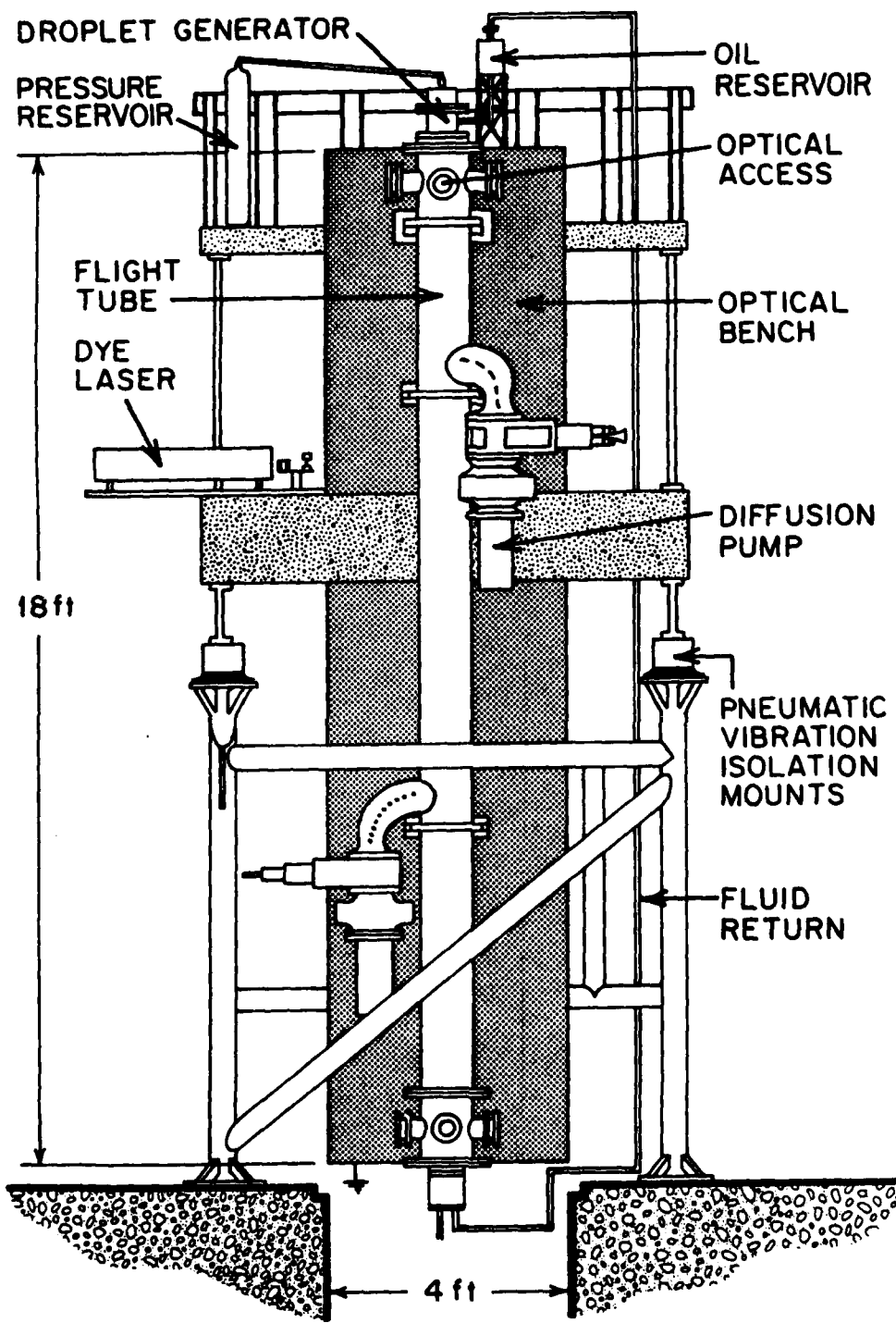


Fig. 1. Sketch of Droplet Dynamics Space Simulator (D^2S^2).

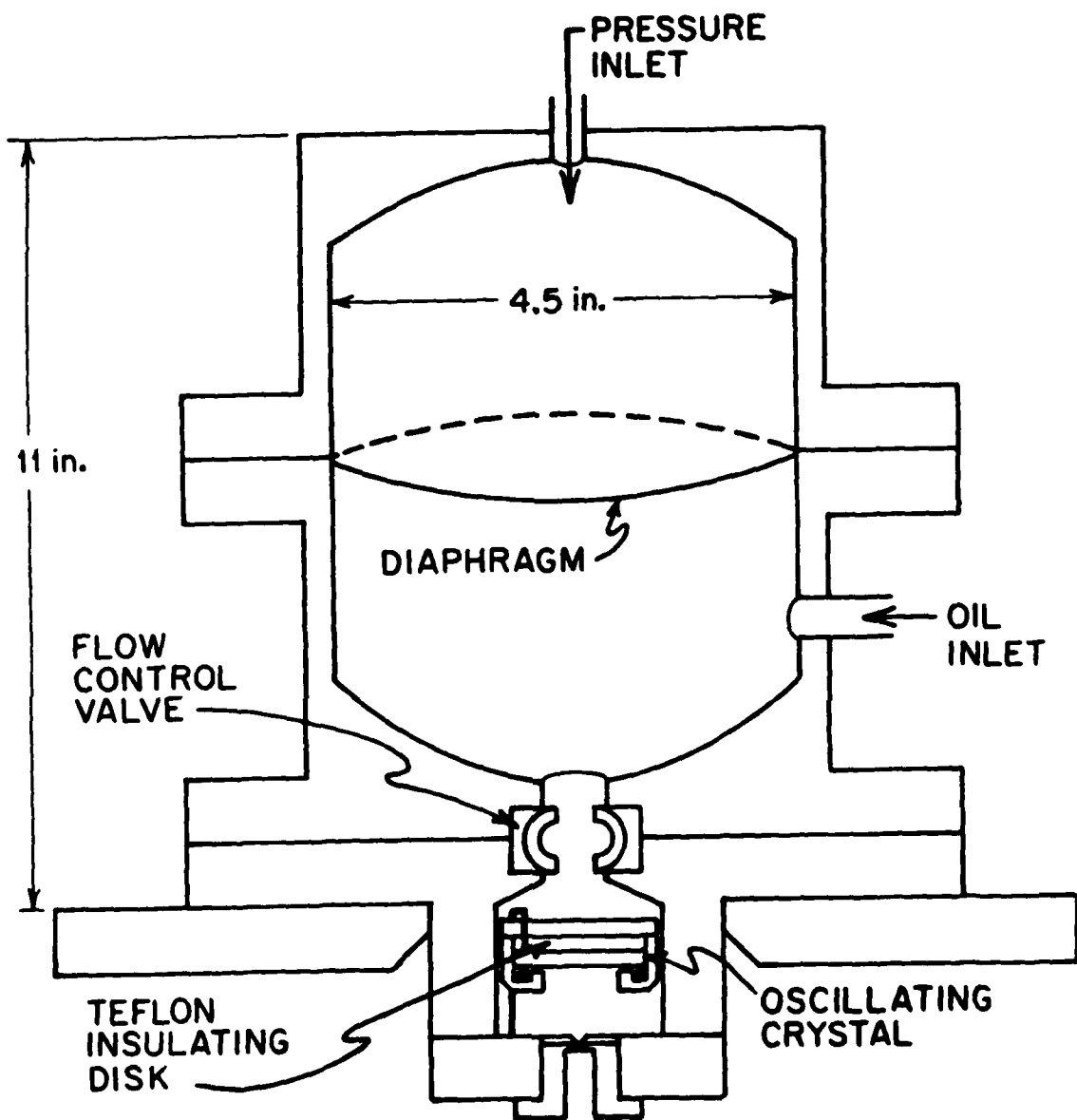


Fig. 2. Schematic of droplet generator.

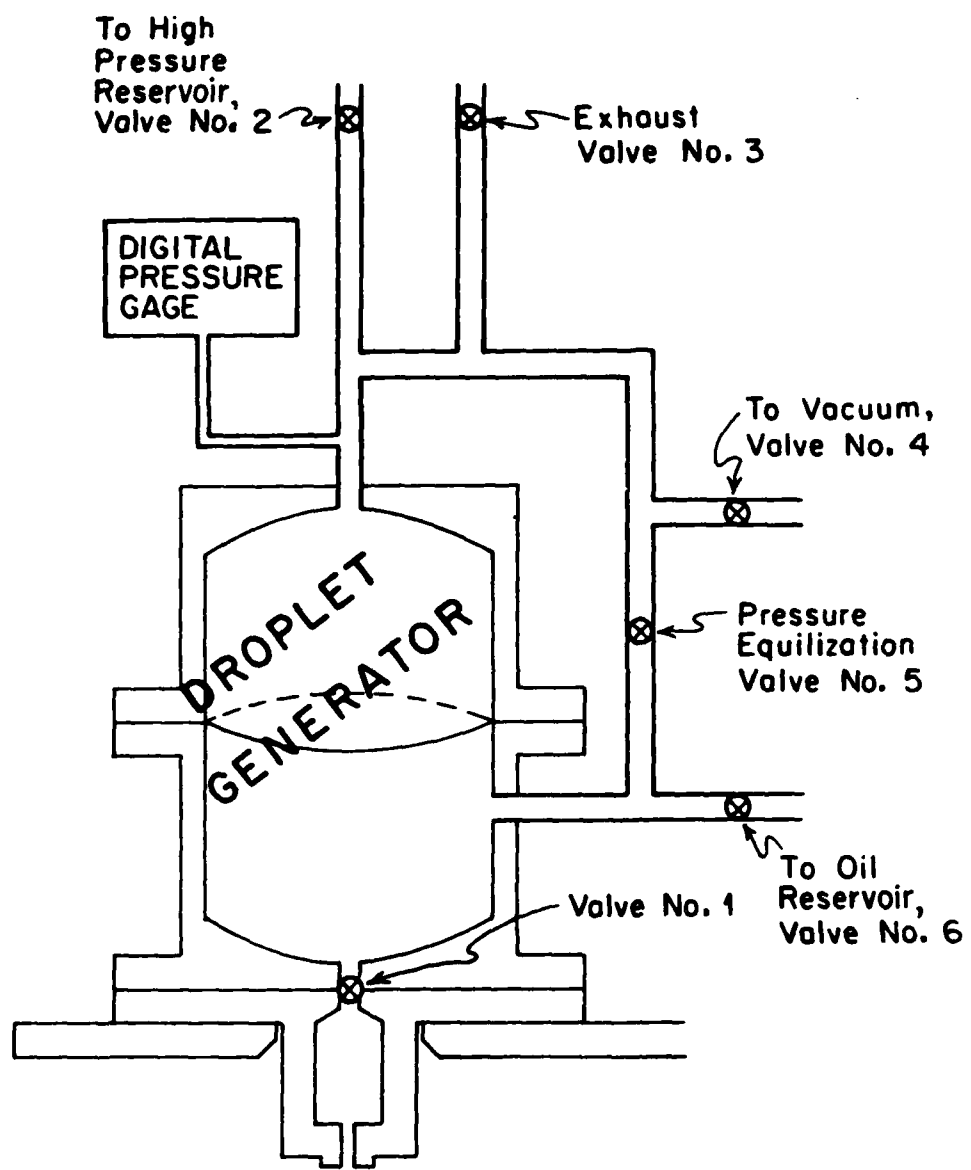


Fig. 3. Operational schematic of droplet generator.

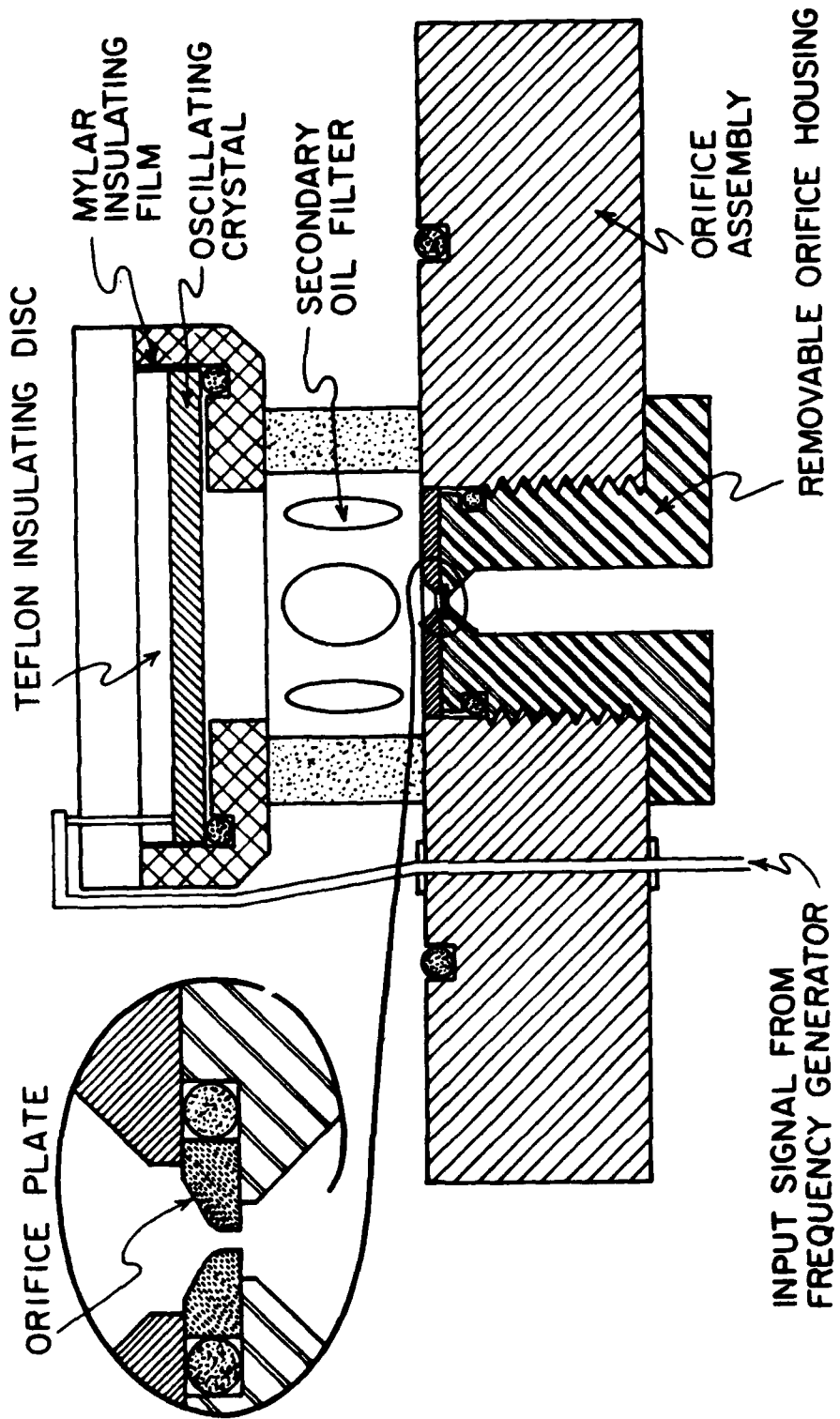


Fig. 4. Orifice and mounting details including oscillator.

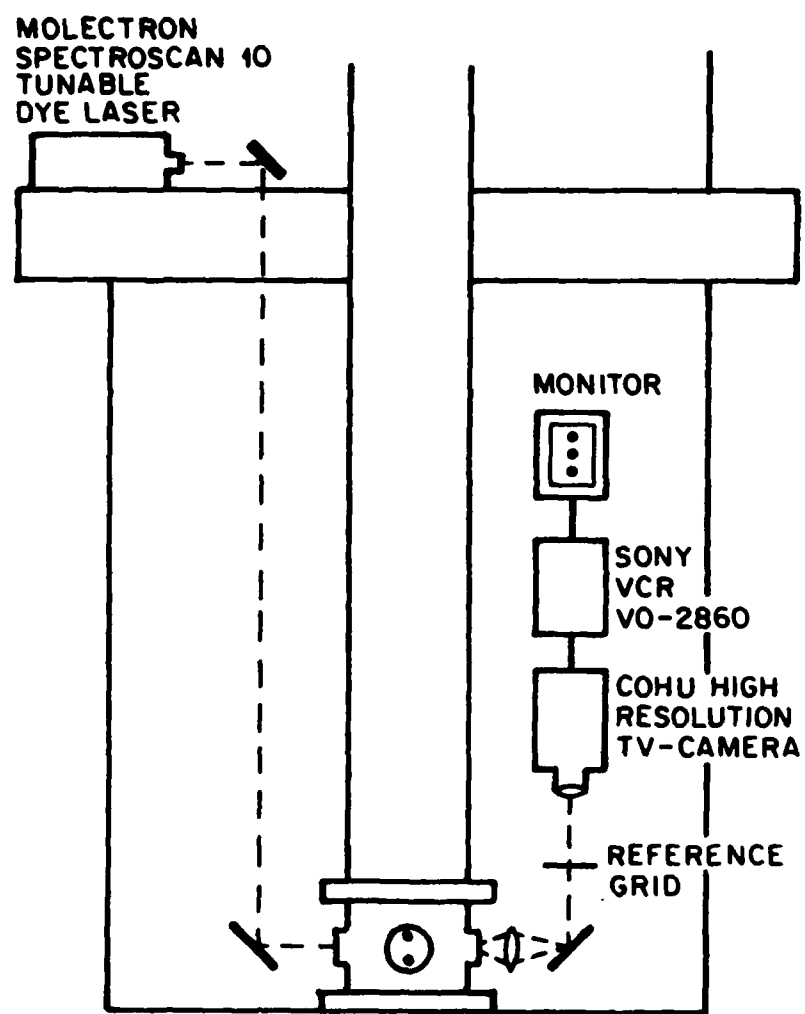


Fig. 5. Schematic of droplet imaging system capable of up to 20 independent images per second with 10^{-8} s exposure time.

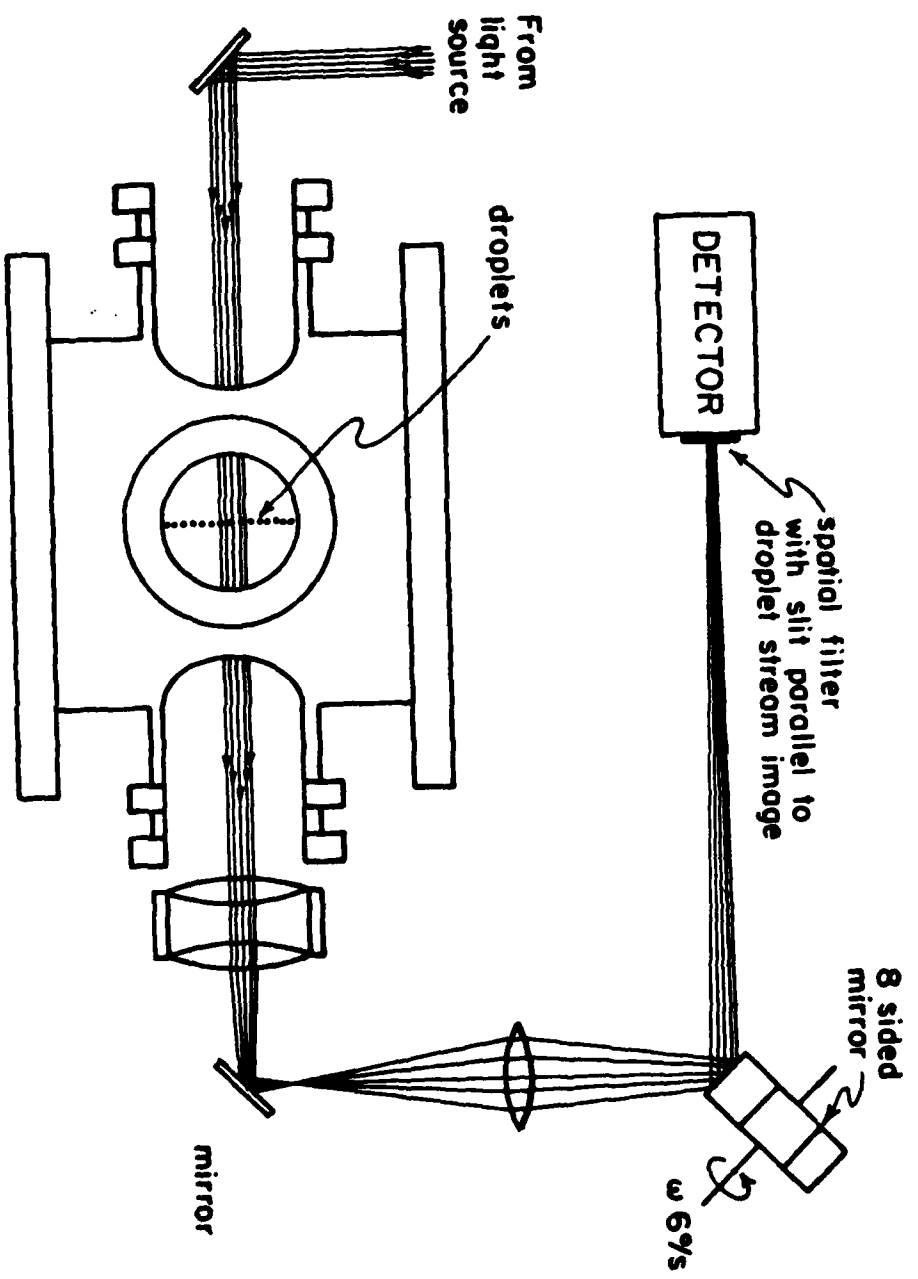


Fig. 6. Schematic of instrument for directly obtaining a measure of droplet stream lateral dispersion over variable time intervals.

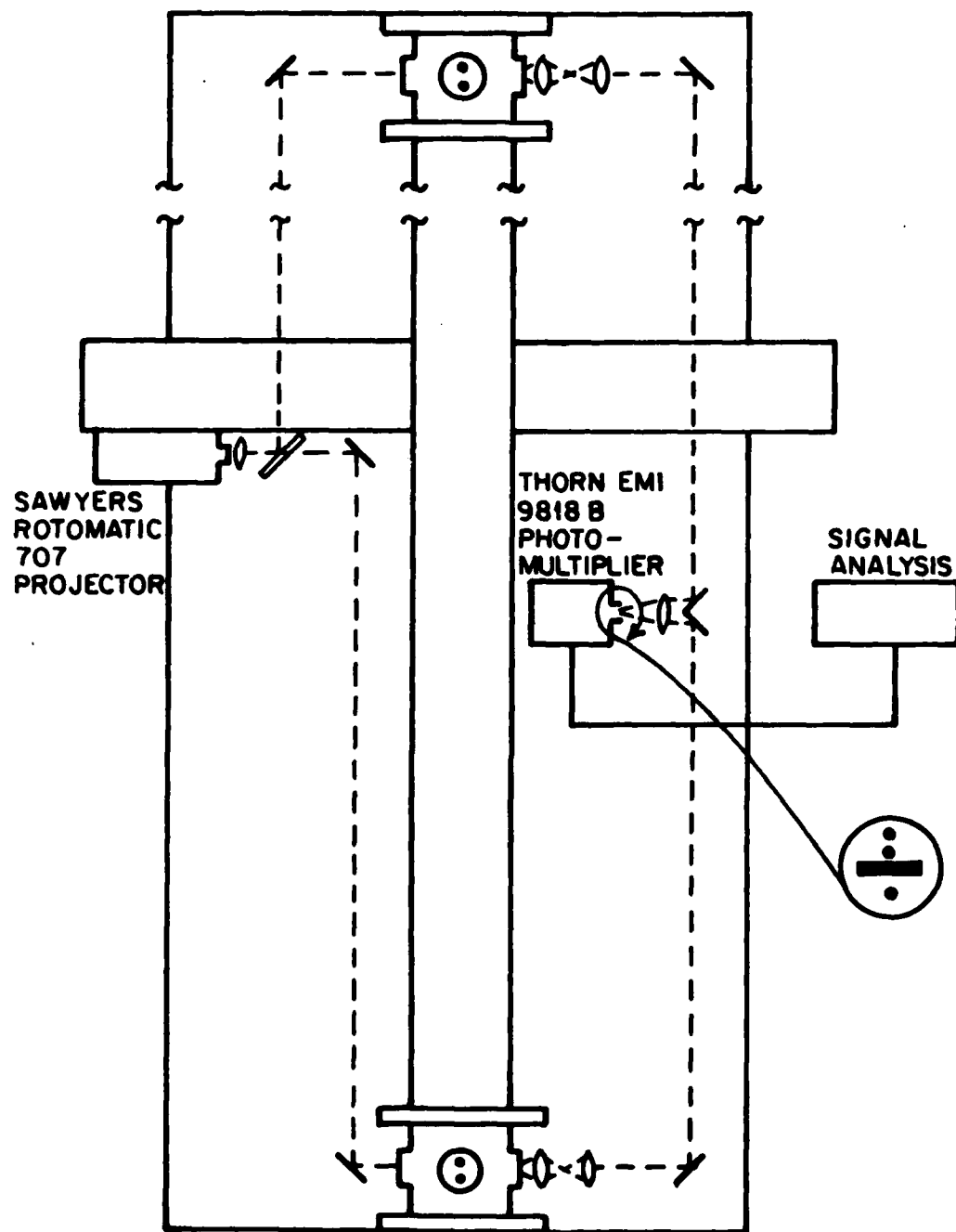


Fig. 7. Schematic of droplet velocimeter.

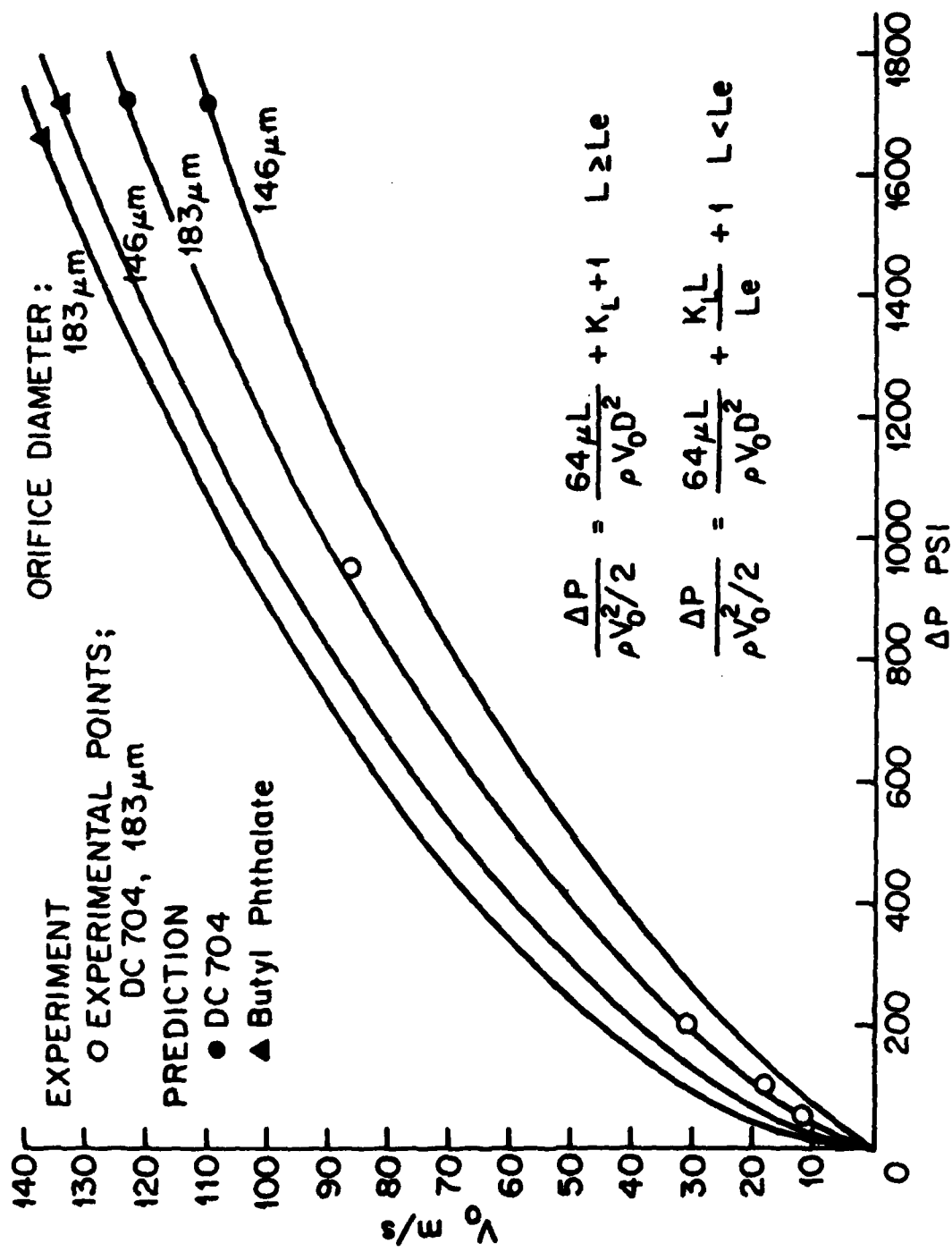


Fig. 8. Average stream speed calculations with experimental comparison.

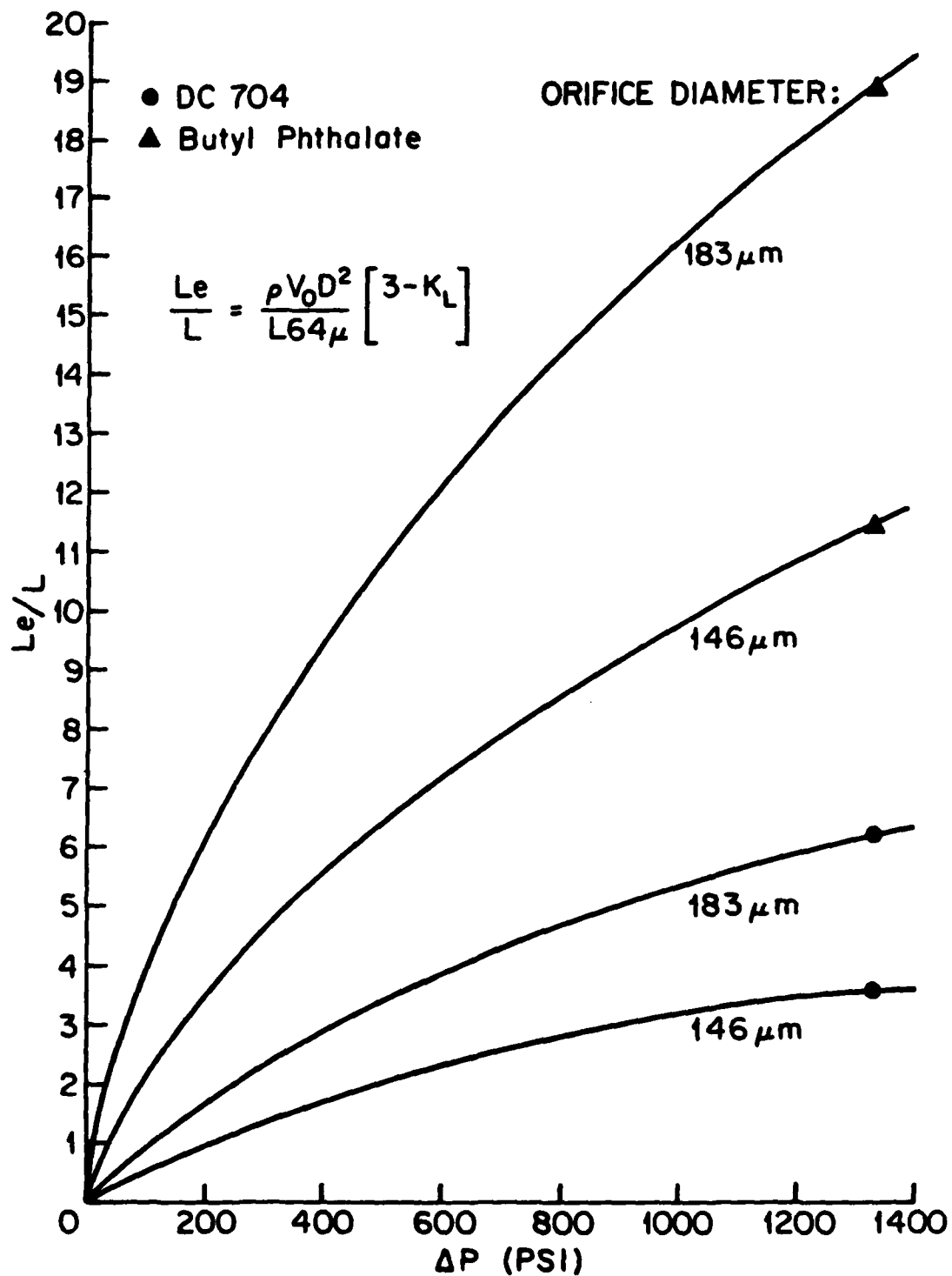


Fig. 9. Entrance lengths compared to nozzle tube length L.

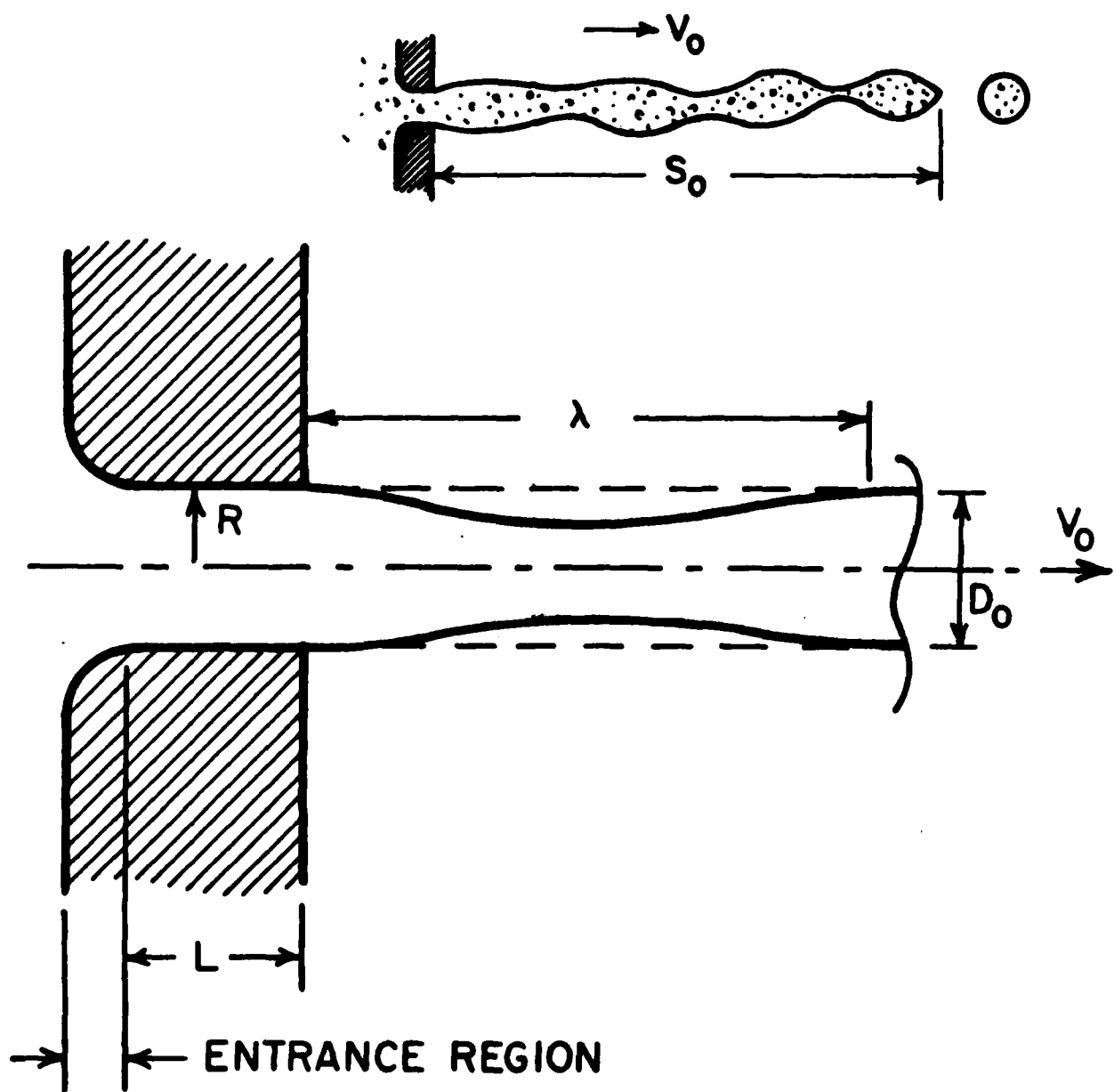


Fig. 10. Nomenclature for capillary stream break-up.

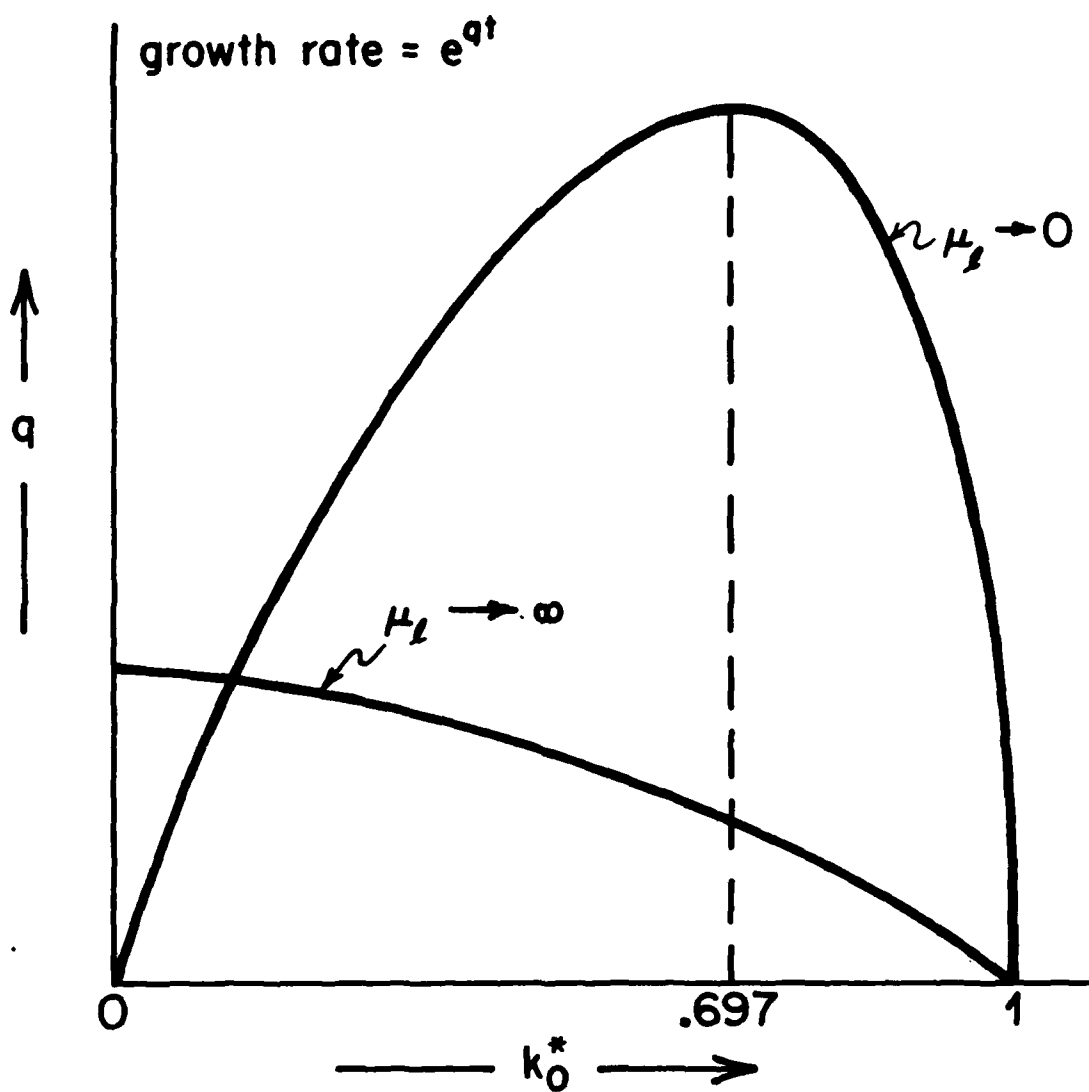


Fig. 11. Capillary column disturbance growth rates as a function of non-dimensional wavenumber of the disturbance.

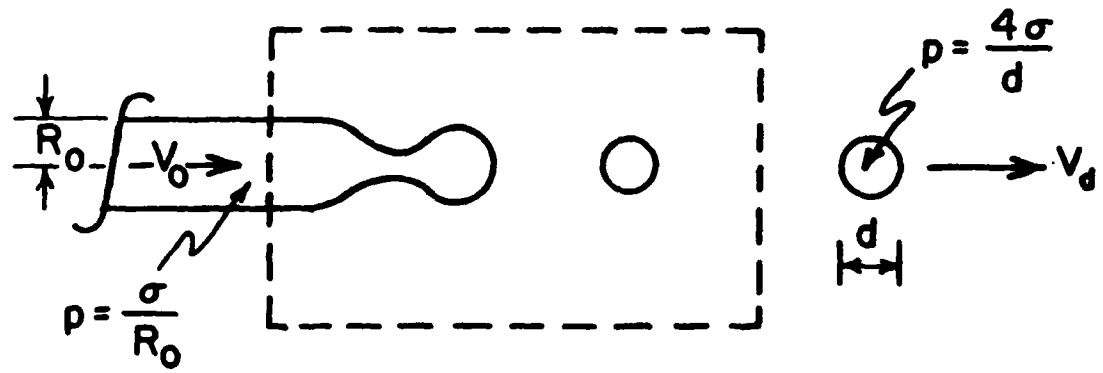


Fig. 12. Control volume for droplet speed calculation.

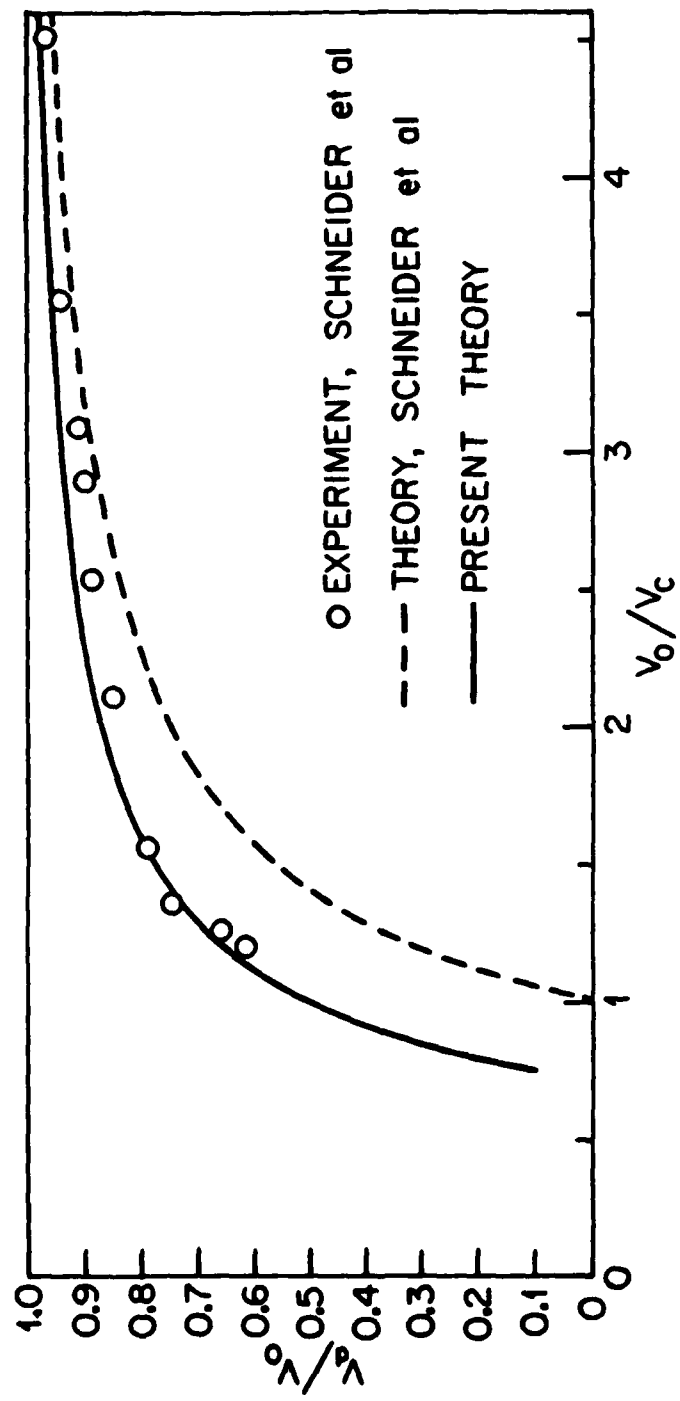


Fig. 13. Comparison of droplet speed data of Schneider et al. (Ref. 11) to eqn. (15) and theory of Schneider et al. (Ref. 10).

SATELLITES: FORMATION AND MERGING

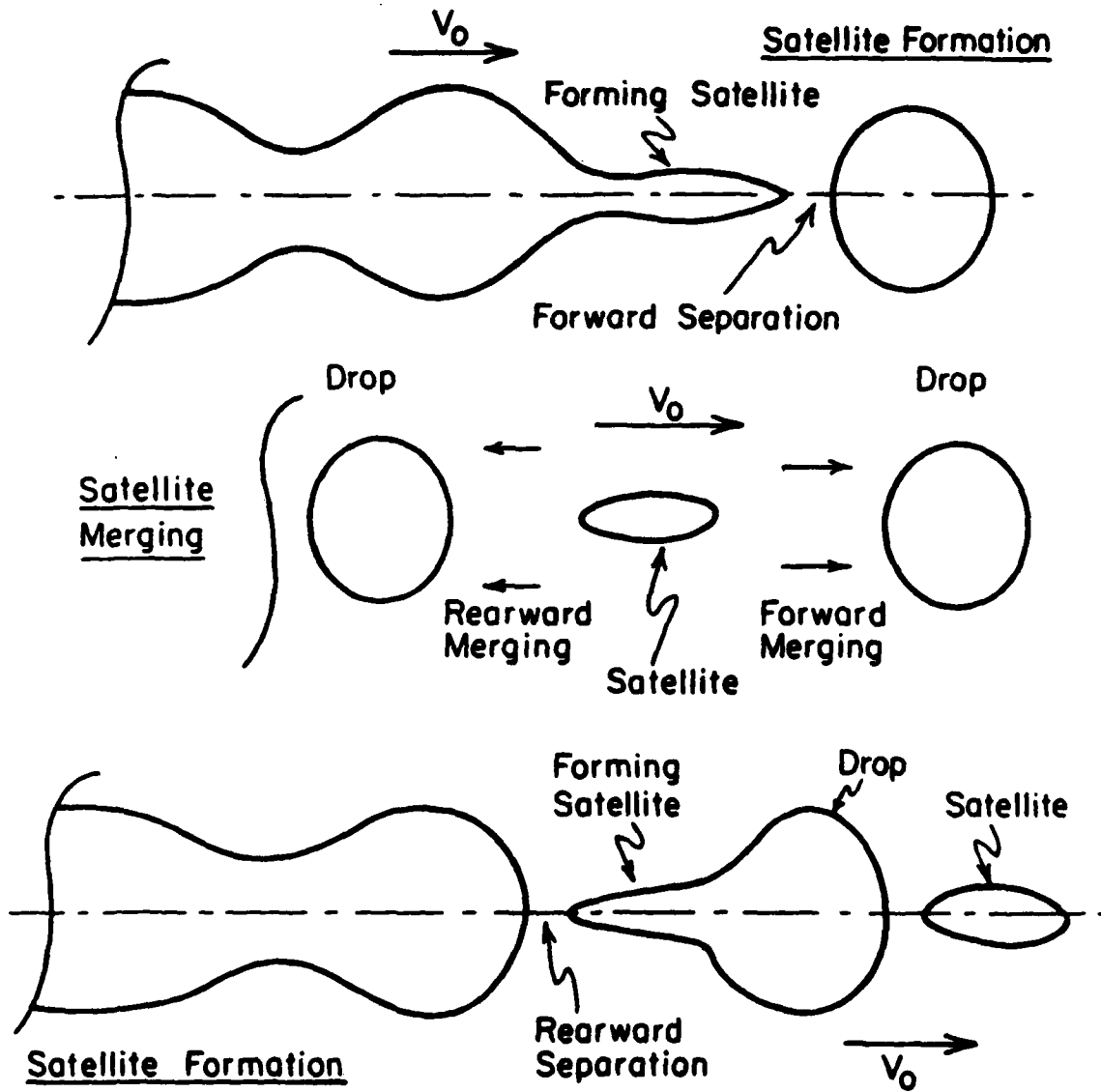
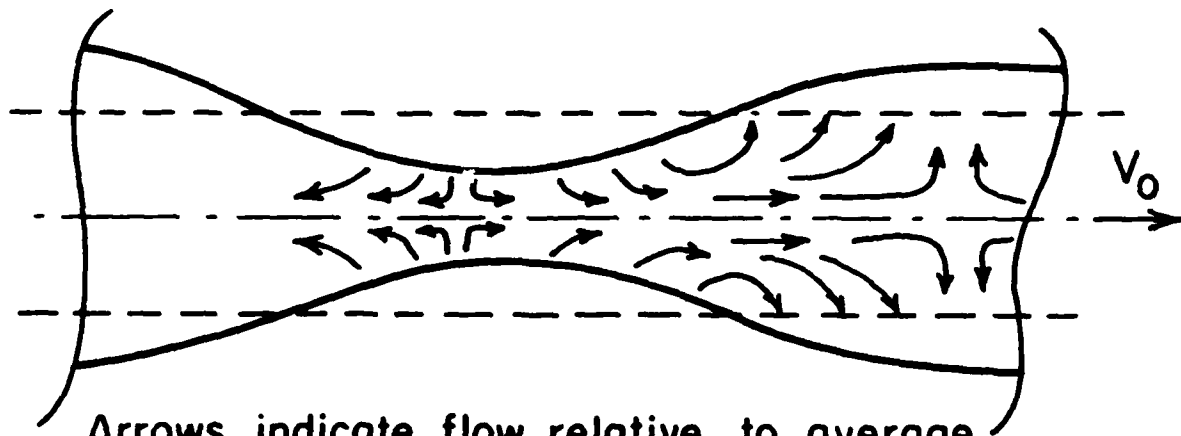
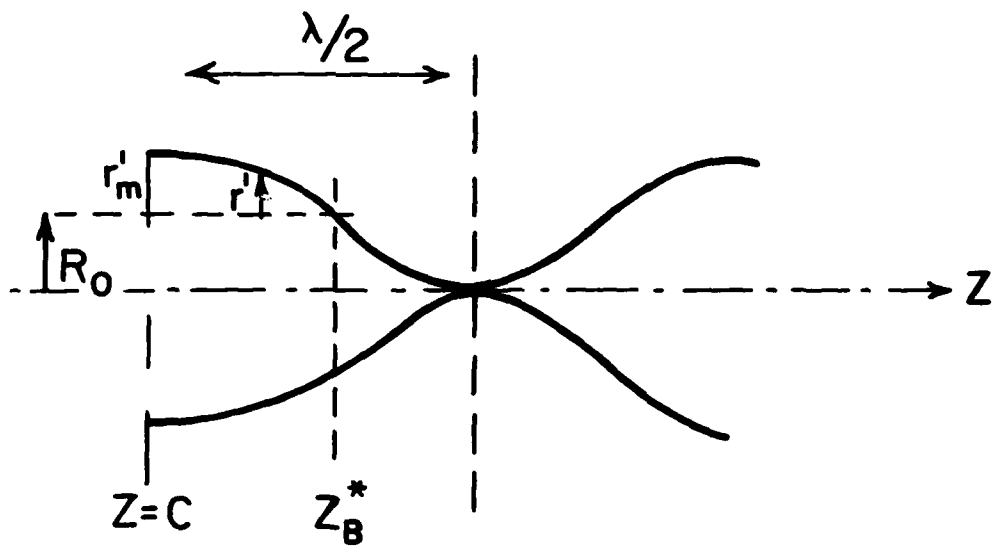


Fig. 14. Schematic of satellite formation and merging terminology.



Arrows indicate flow relative to average speed V_0 .

Fig. 15. Co-ordinate system and nomenclature for calculation of perturbation momentum.

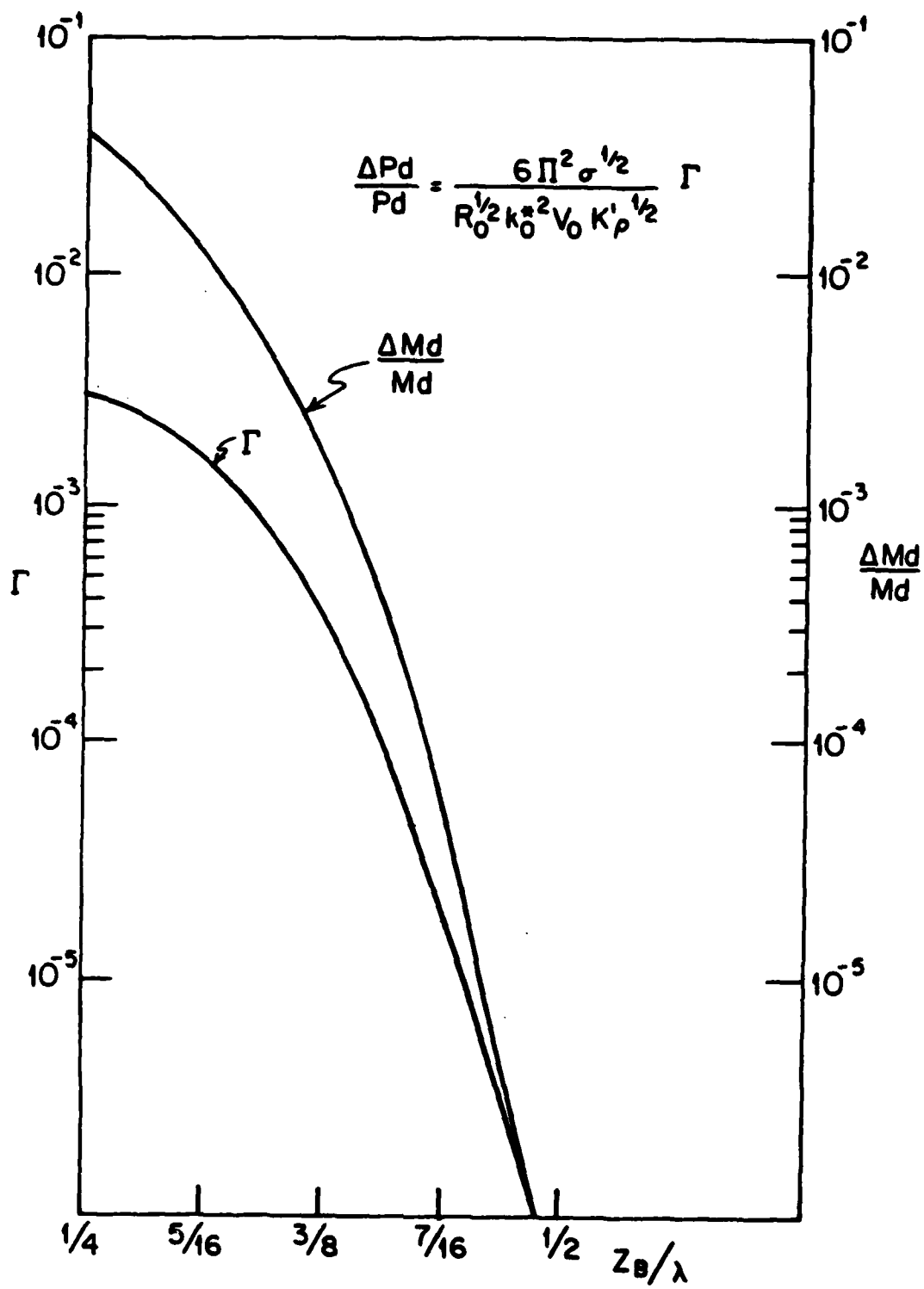


Fig. 16. Functions for determining momentum and mass perturbation for a range of non-dimensional break-off position, Z_B/λ .

EXTERNAL FORCES ON STREAM

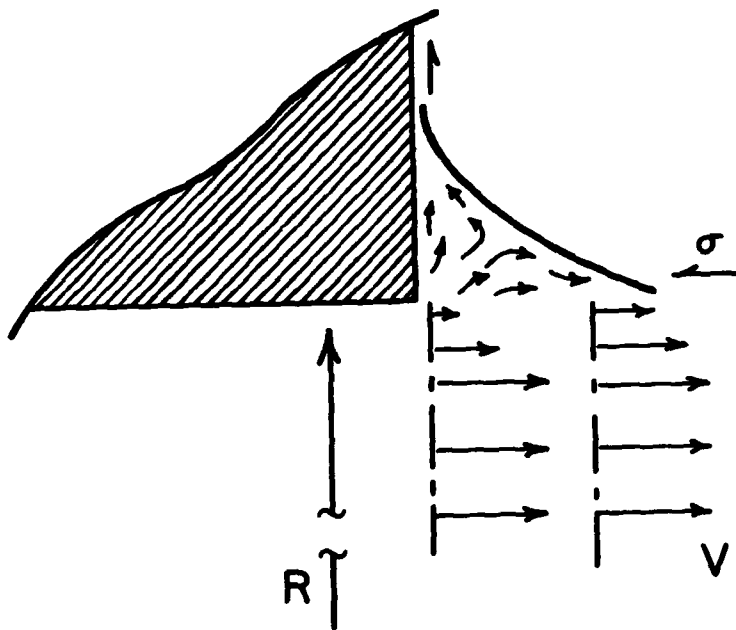
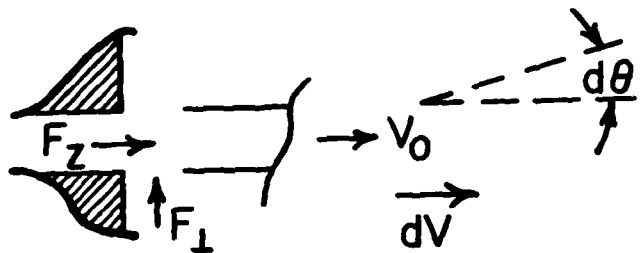


Fig. 17. Schematic of stream as an isolated body and hypothetical exit surface flow configurations.

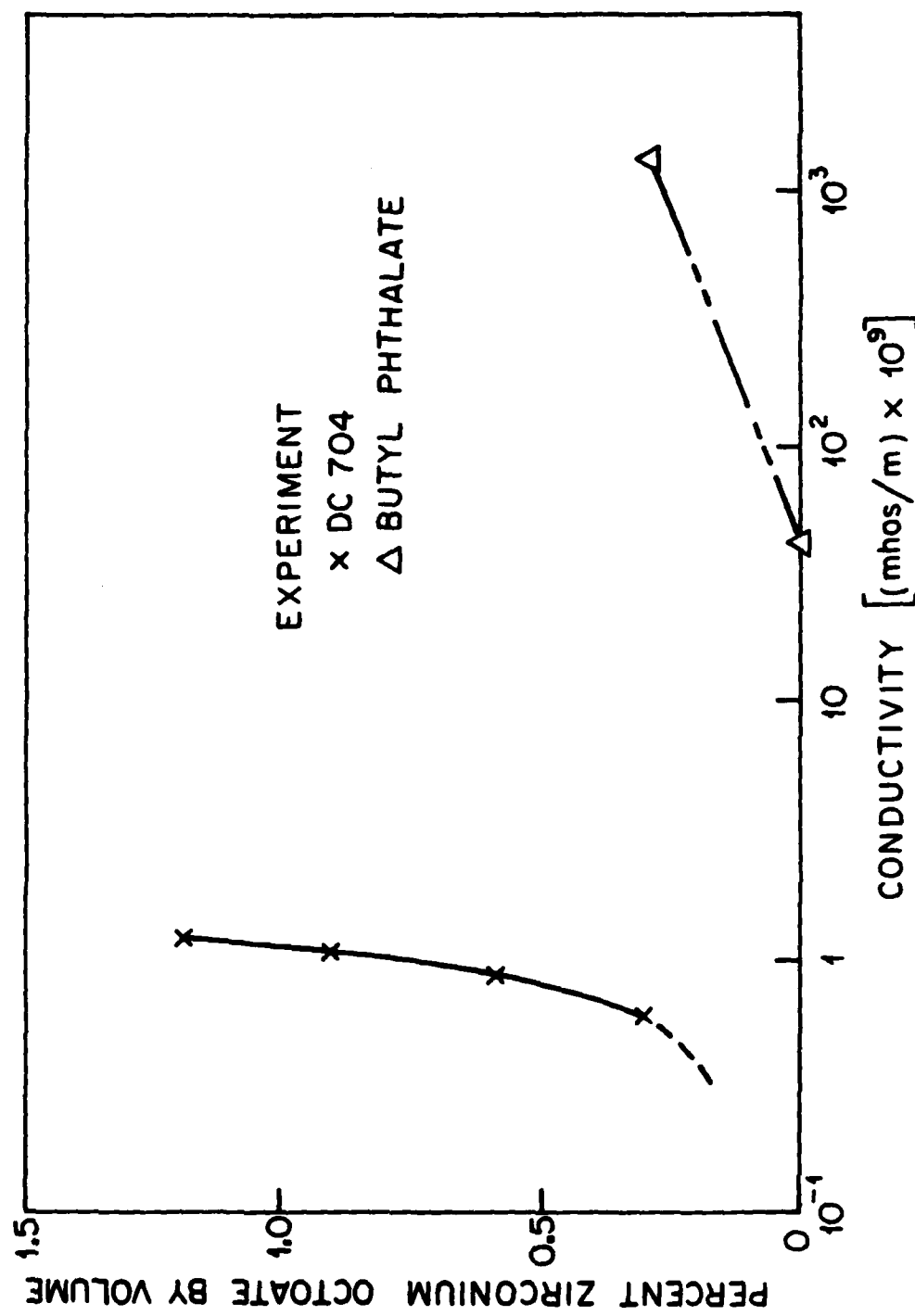


Fig. 18. Measured conductivities of liquids used in the experiments and the effect of an additive.

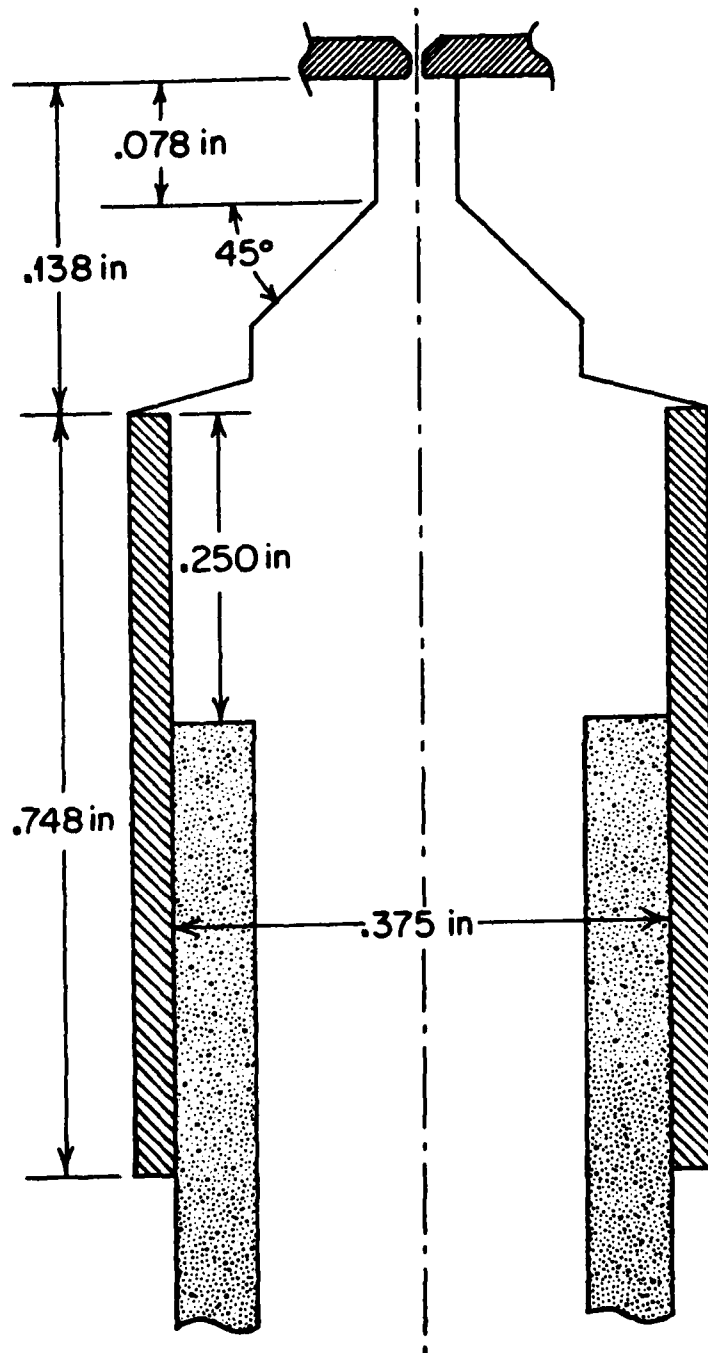


Fig. 19. Charging electrode configuration.

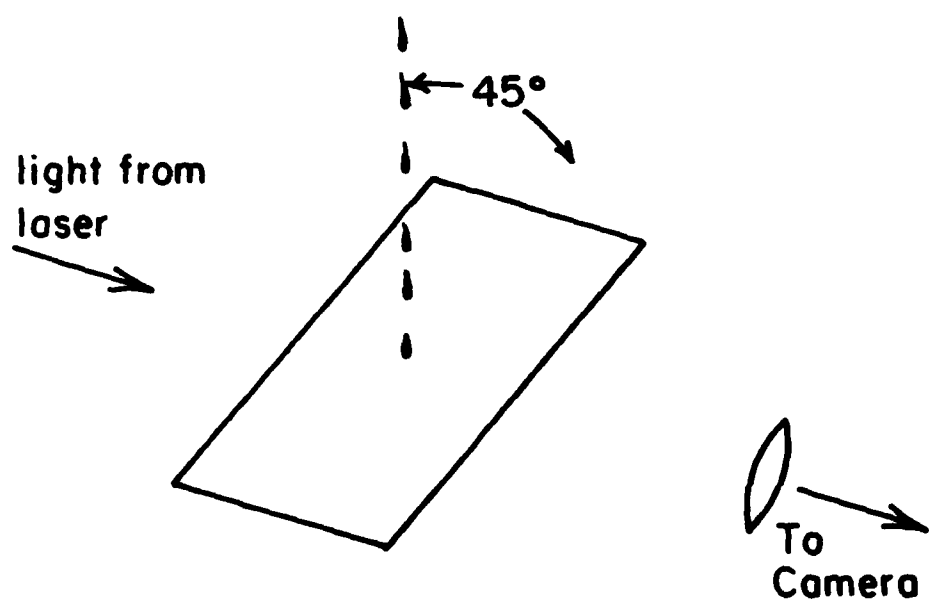


Fig. 20. Schematic of plate impact experiment.

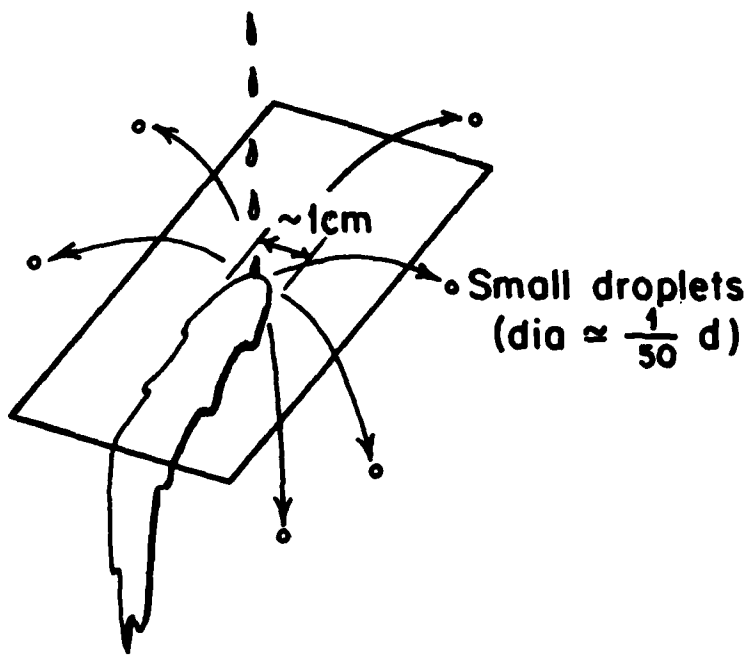


Fig. 21. Sketch of plate impact flow field.

END

FILMED

10-84

DTIC